Electronic supplementary materials *Mendeleev Commun.*, 2020, **30**, 220–222

TiO_2-modified MALDI target for *in vitro* modeling of the oxidative biotransformation of diclofenac

Alexander Yu. Gorbunov, Konstantin A. Krasnov, Alexander A. Bardin, Olga A. Keltsieva, Vladimir N. Babakov and Ekaterina P. Podolskaya

Contents

Electrochemical oxidation of diclofenac. 80 mL of 31.43 μmol dm^{-3} diclofenac solution in a 50/50 (v/v) mixture of 20 mmol dm^{-3} ammonium formiate and acetonitrile (Merck Millipore) was loaded into a SynthesisCell reactor equipped with a Magic Diamond (boron doped diamond) working electrode (Antec Scientific) controlled via a high current ROXY Potentiostat (Antec Scientific); a working potential of +1.5 V was applied for 60 min.

Bulk UV/TiO_2-PCO of diclofenac. The procedure was performed in a 100 mL quartz flask placed in a lab-made photoreactor equipped with a magnetic stirrer and eight UVA lamps (9W, 365 nm) at the inner perimeter of a reaction chamber. Suspension of 1 mg/mL TiO_2 nanopowder (Sigma; particle size, 21 nm) in 31.43 μmol dm^{-3} aqueous solution of diclofenac was sonicated in an ultrasound batch for 10 min and then UV-irradiated for 15 min at 20°C with intense stirring. After photocatalytic oxidation, 1 mL aliquot portionss of the suspension were clarified by centrifugation (10 000g, 10 min), and the supernatants were filtered through Millex Samplicity 0.2 μm filters (Merck Millipore) to remove residual nanoparticles.

On-target UV/TiO2-PCO. Nanopowder TiO_2 layer was formed by applying 1.5 μL droplets of 100 μg/mL TiO_2 aqueous suspension onto sample spots of MTP 384 MALDI target (Bruker Daltonics) followed by drying at room temperature. After cooling the MALDI target down to 4°C, 1 μL droplets of 10 μg/mL (31.43 μM) aqueous solution of diclofenac were applied to TiO_2 spots. UV/TiO_2-PCO was performed by irradiating the MALDI target with a UVA lamp (9W, 365 nm) at a 40 mm distance for 30 min. Dried samples were either left untreated or covered with a MALDI matrix solution. The following MALDI matrices were used: 2,5-dihydroxybenzoic acid (DHB), 9-aminoacridine, *meso*-tetrakis(pentafluorophenyl)porphyrin, norharmane, alpha-cyano-4-hydroxycinnamic acid (CHCA), and 2,6-dihydroxyacetophenone. The MALDI-FT-ICR MS analysis was performed using SolariX XR 7T equipped with a Smartbeam-II Nd:YAG laser (355 nm) (Bruker Daltonics) in a positive or negative ion mode. MALDI parameters were as follows: laser pulse repetition rate, 1 kHz; laser power, 60%; 200 shots per scan, medium laser focus. Mass spectra were recorded in a range of *m/z* 150-600 with 16 scans accumulated for each spectrum. The electrochemical and photocatalytic oxidation products were analyzed by FT-ICR MS using SolariX XR 7T (Bruker Daltonics) with direct sample injection into an ESI ion source at an injection rate of 2 μL/min and a capillary voltage of 4.5kV. Analysis was performed in the negative ion mode, and the mass spectra were collected in a range of *m/z* 150–600.

HPLC-MS/MS analysis of electrochemical and photocatalytic oxidation products. 5 μL samples were injected into a 1260 Infinity HPLC system (Agilent Technologies) with a Chromolith Performance RP-18e 100-2 mm column (Merck) connected to a SolariX XR 7T ESI ion source. HPLC was performed at a flow rate of 200 μL/min using acetonitrile and 10 mM aqueous ammonium formate (pH 7.4) as mobile phases A and B, respectively. The ESI-FT-ICR MS parameters were as follows: a capillary voltage of 4.5kV, a negative ion mode, a scanning range of *m/z* 100–600, fragmentation by collision induced dissociation (CID) using Ar as a collision gas with collision energy set by the instrument, and estimated resolving power of 100 000 at *m/z* 400.

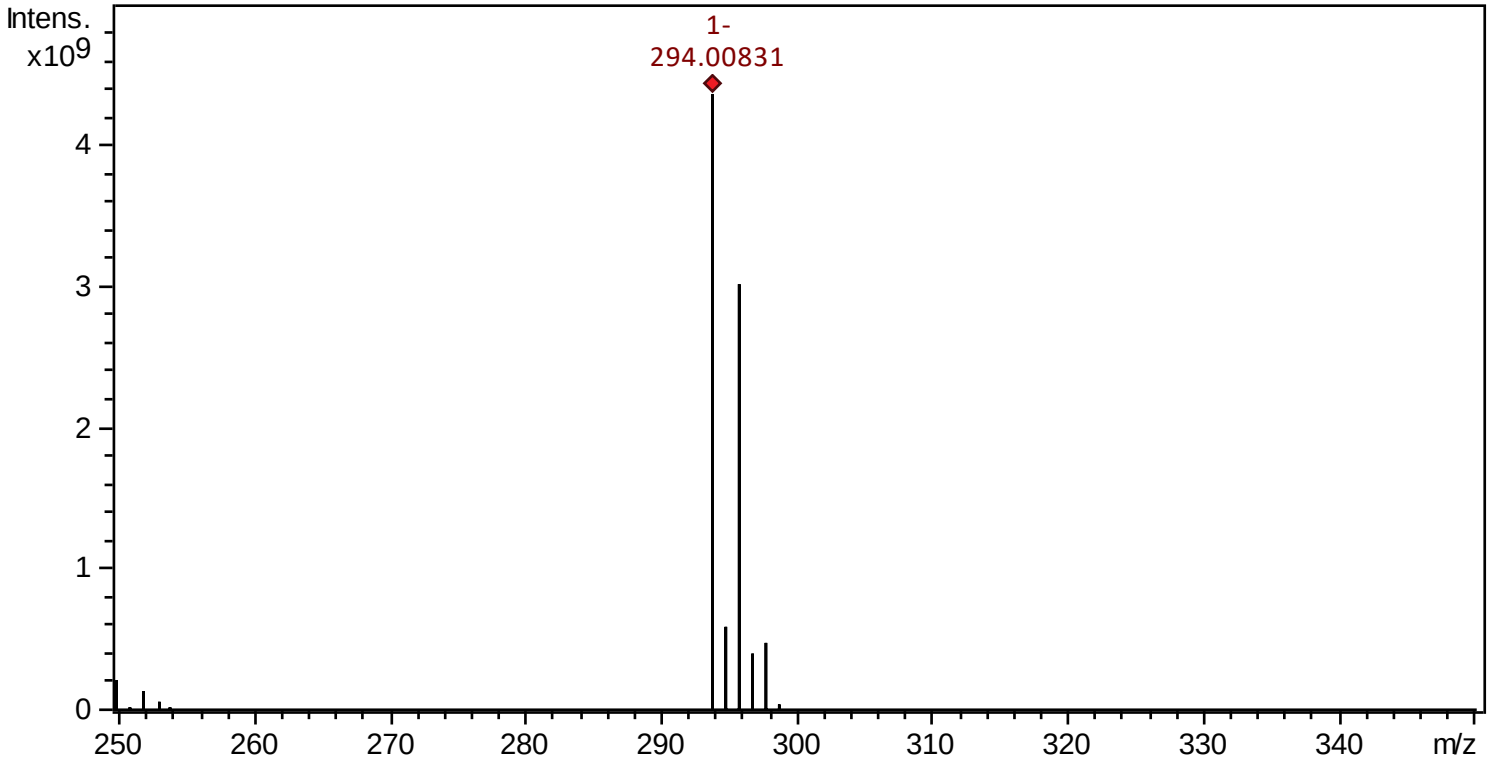

Figure S1. MS spectrum of DCl (m/z 294,0083).

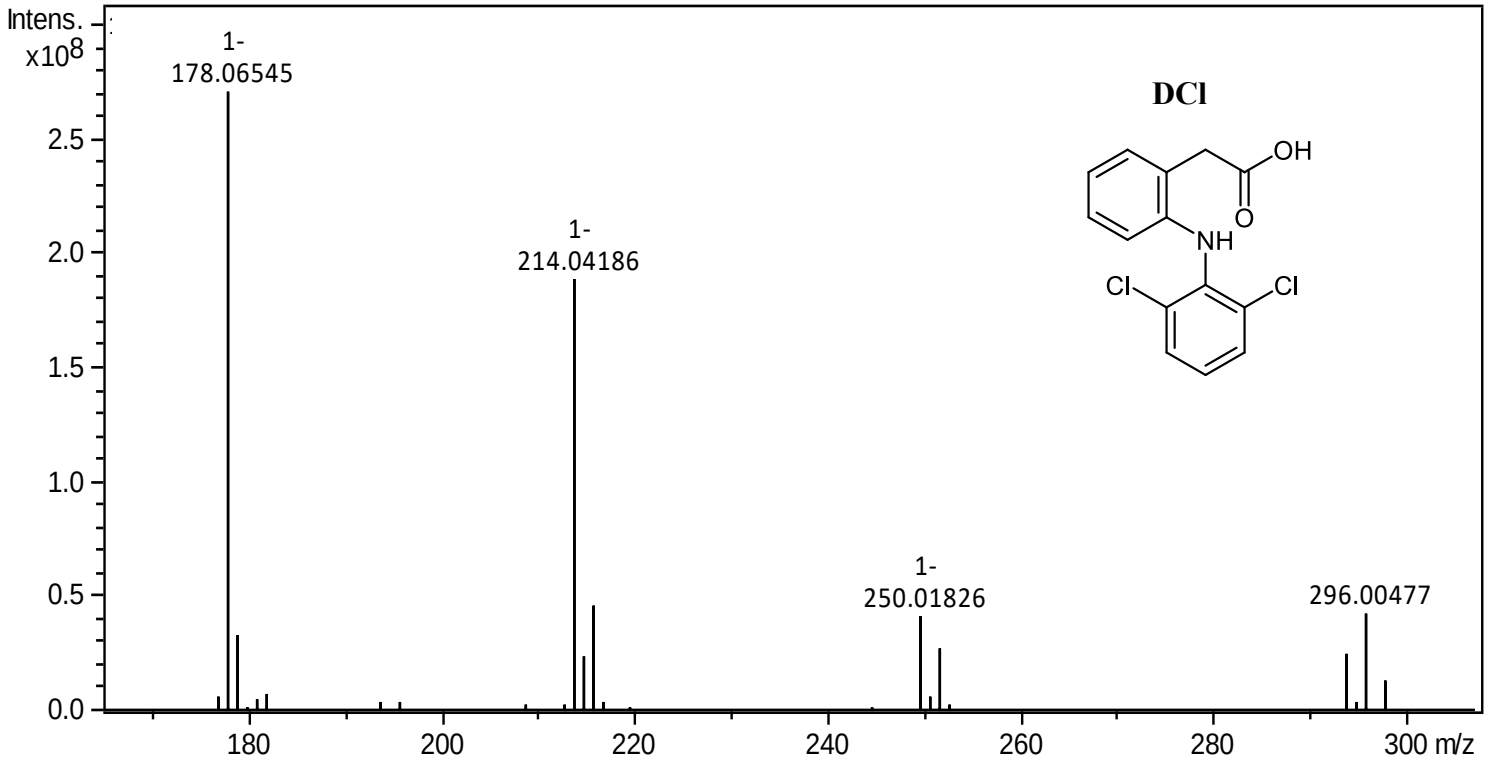

Figure S1a. MS/MS spectrum of DCl precursor ion and its structure.

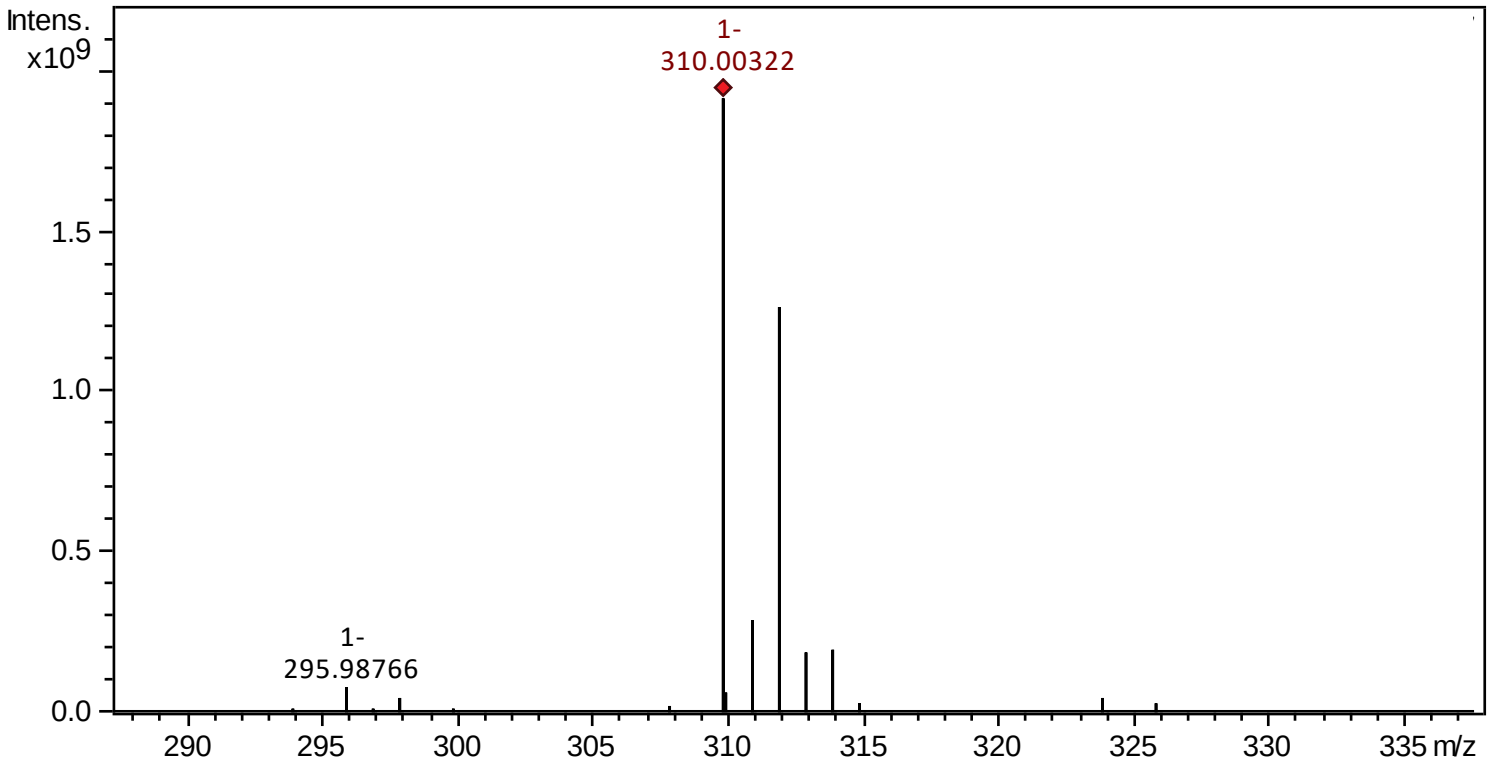

Figure S2. MS spectrum of the oxidation product 2a (m/z 310,0032).

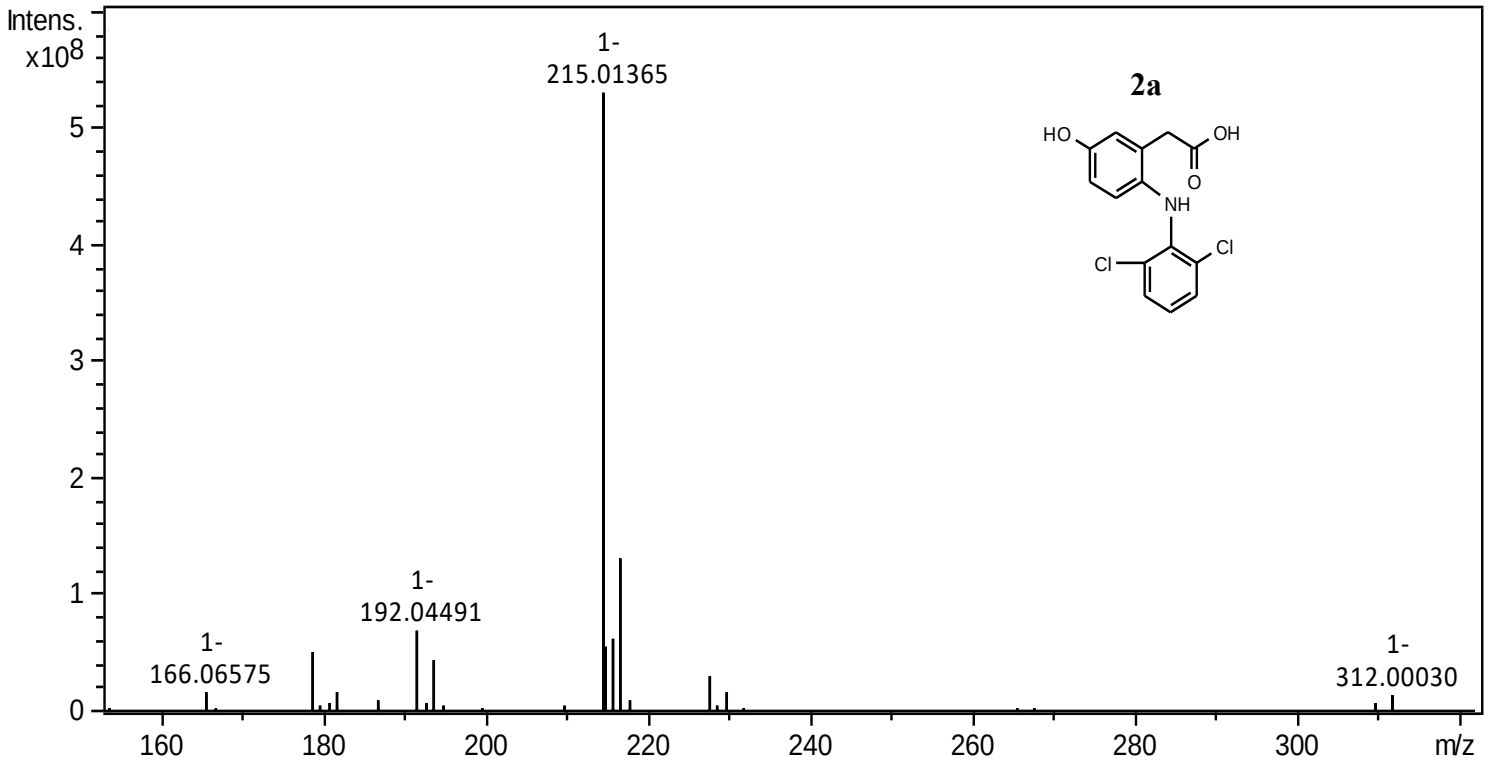

Figure S2a. MS/MS spectrum of 2a precursor ion and its proposed molecular structure.

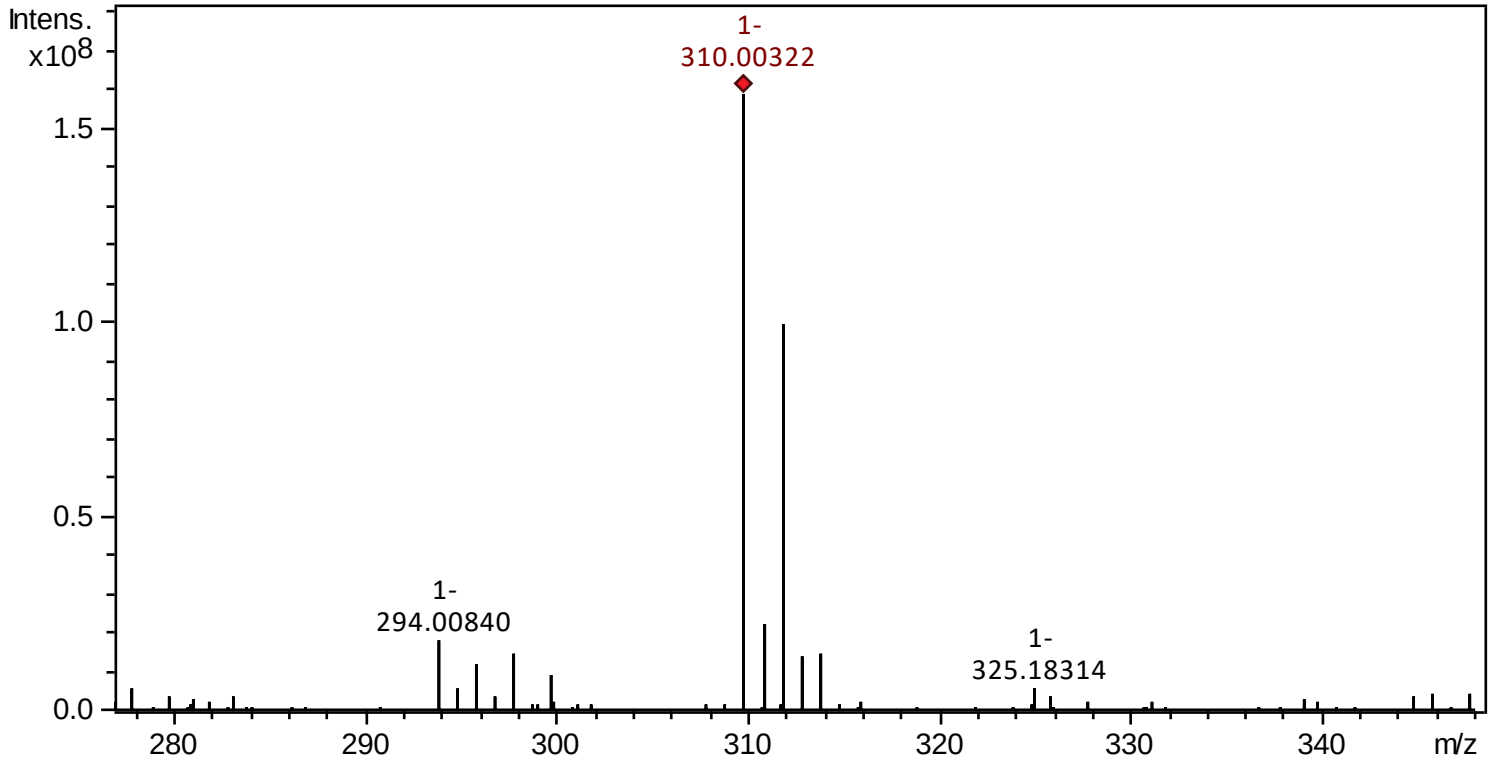

Figure S3. MS spectrum of the oxidation product 2b (m/z 310,0032).

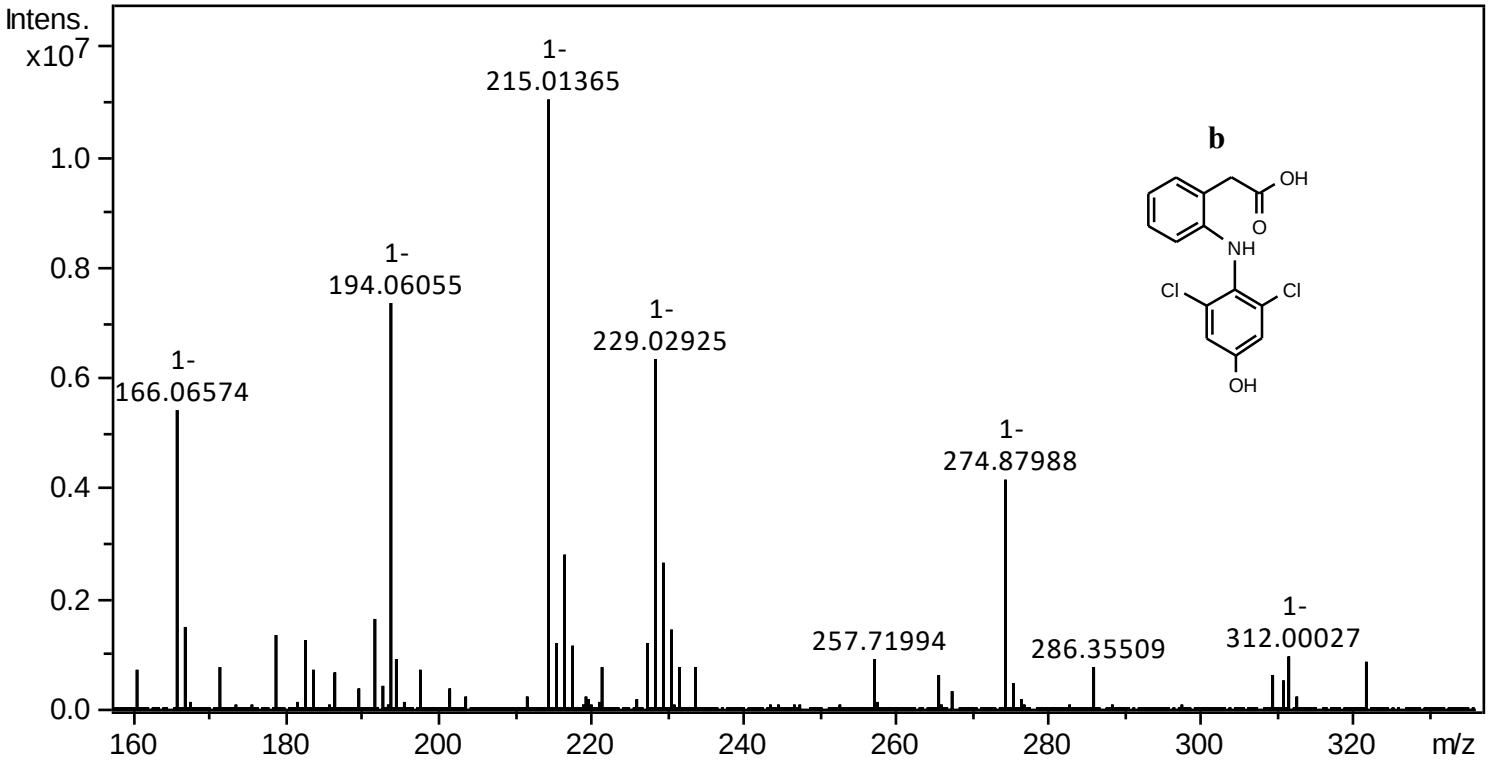

Figure S3a. MS/MS spectrum of 2b precursor ion and its proposed molecular structure.

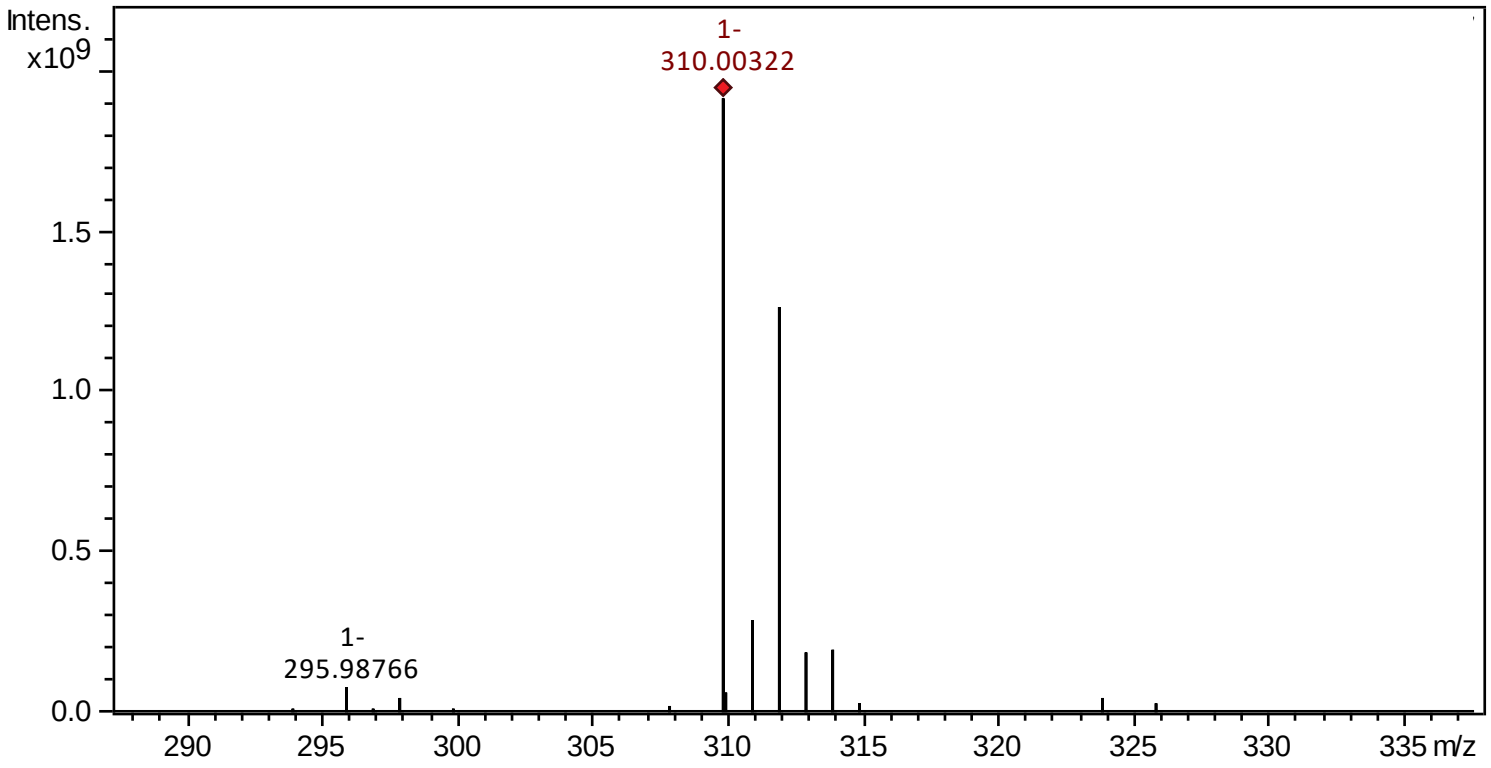

Figure S4. MS spectrum of the oxidation product 2c (m/z 310,0032).

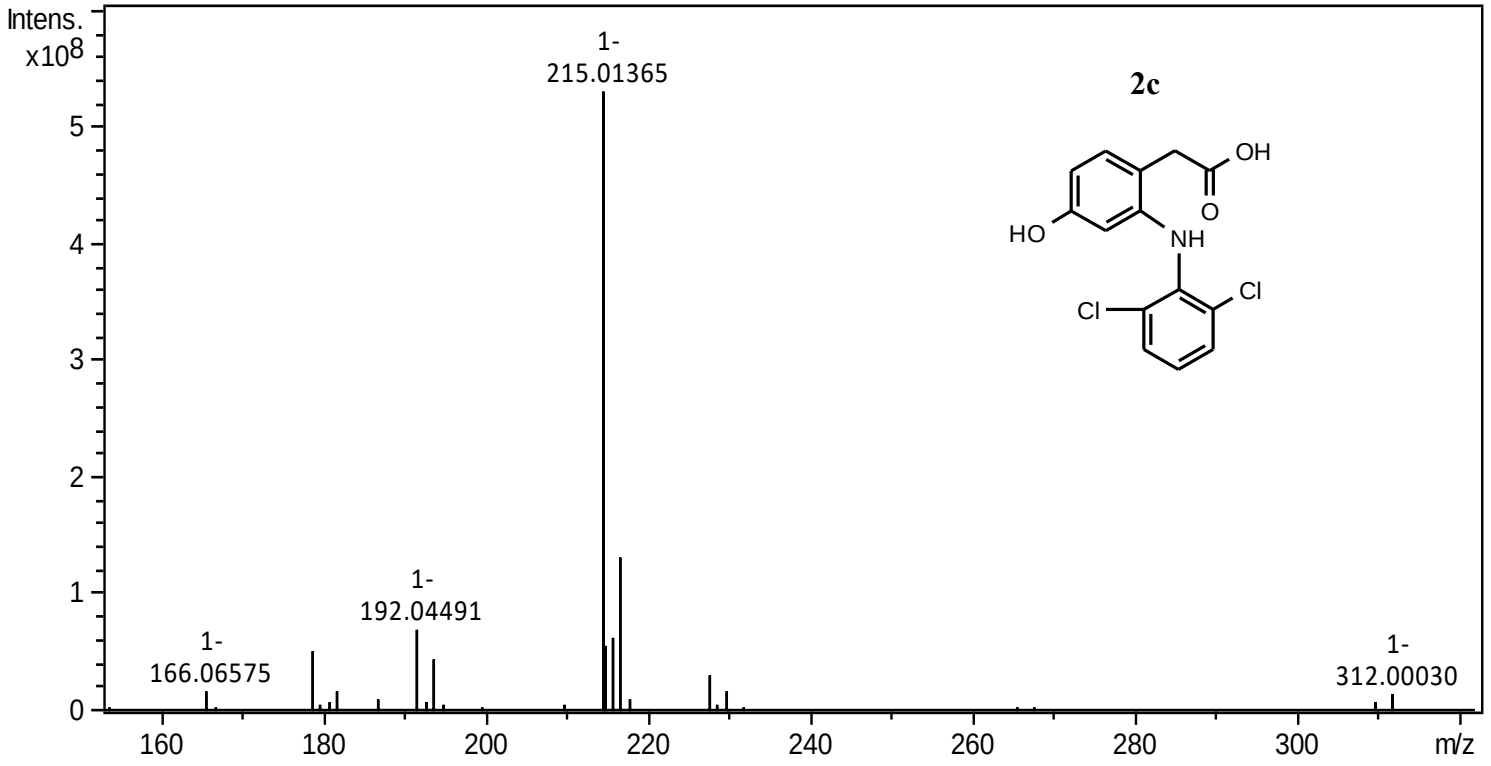

Figure S4a. MS/MS spectrum of 2c precursor ion and its proposed molecular structure.

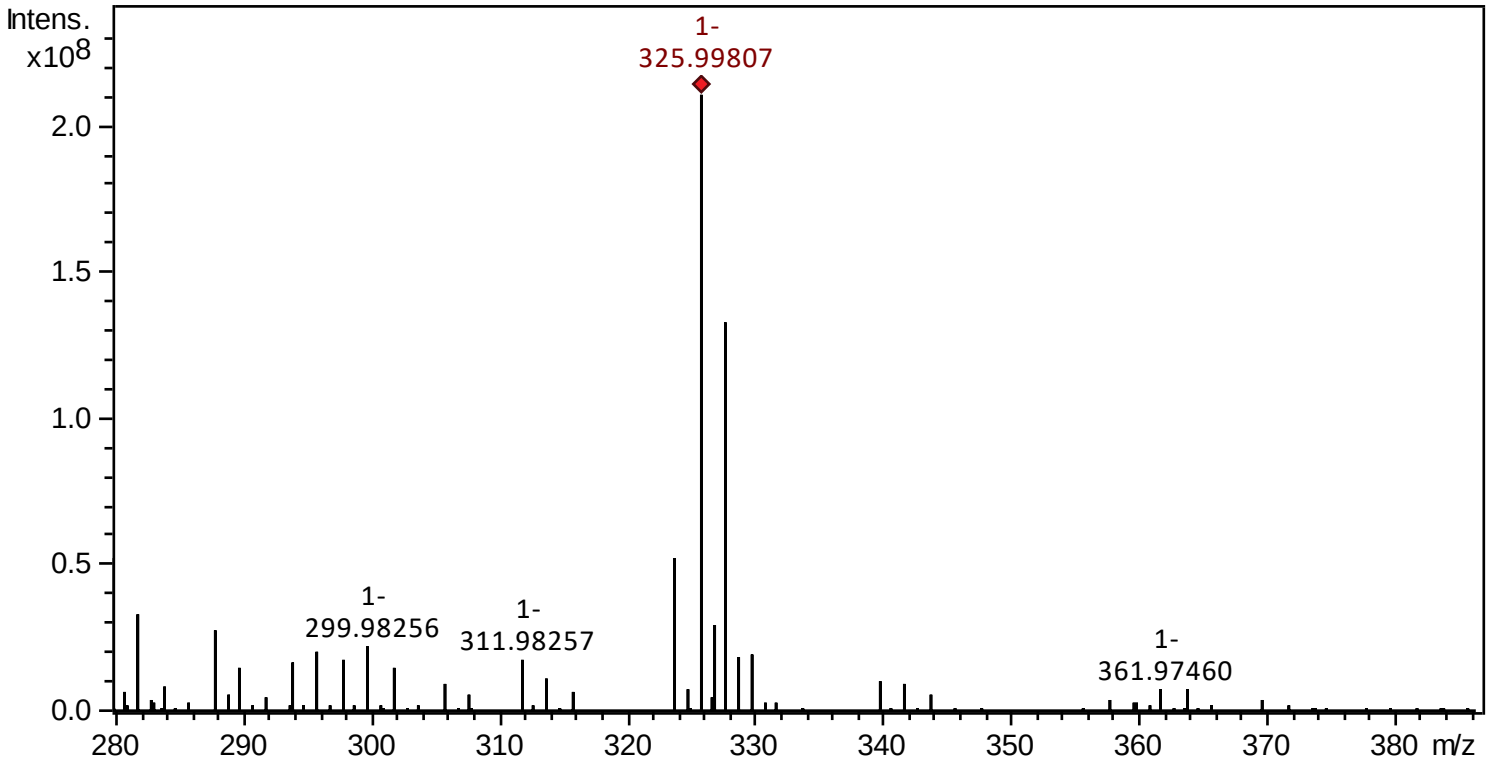

Figure S5. MS spectrum of the oxidation product 2d (m/z 325,9980).

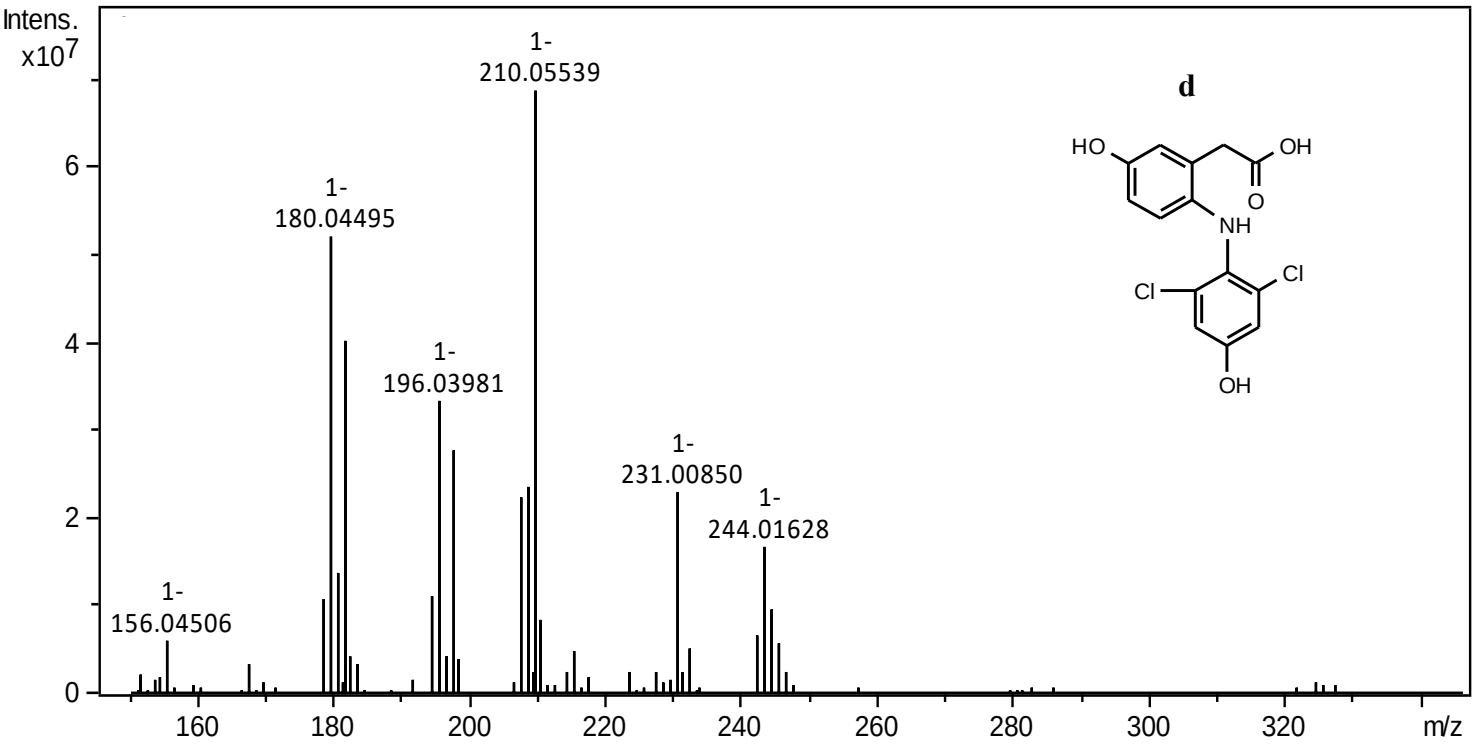

Figure S5a. MS/MS spectrum of 2d precursor ion and its proposed molecular structure.

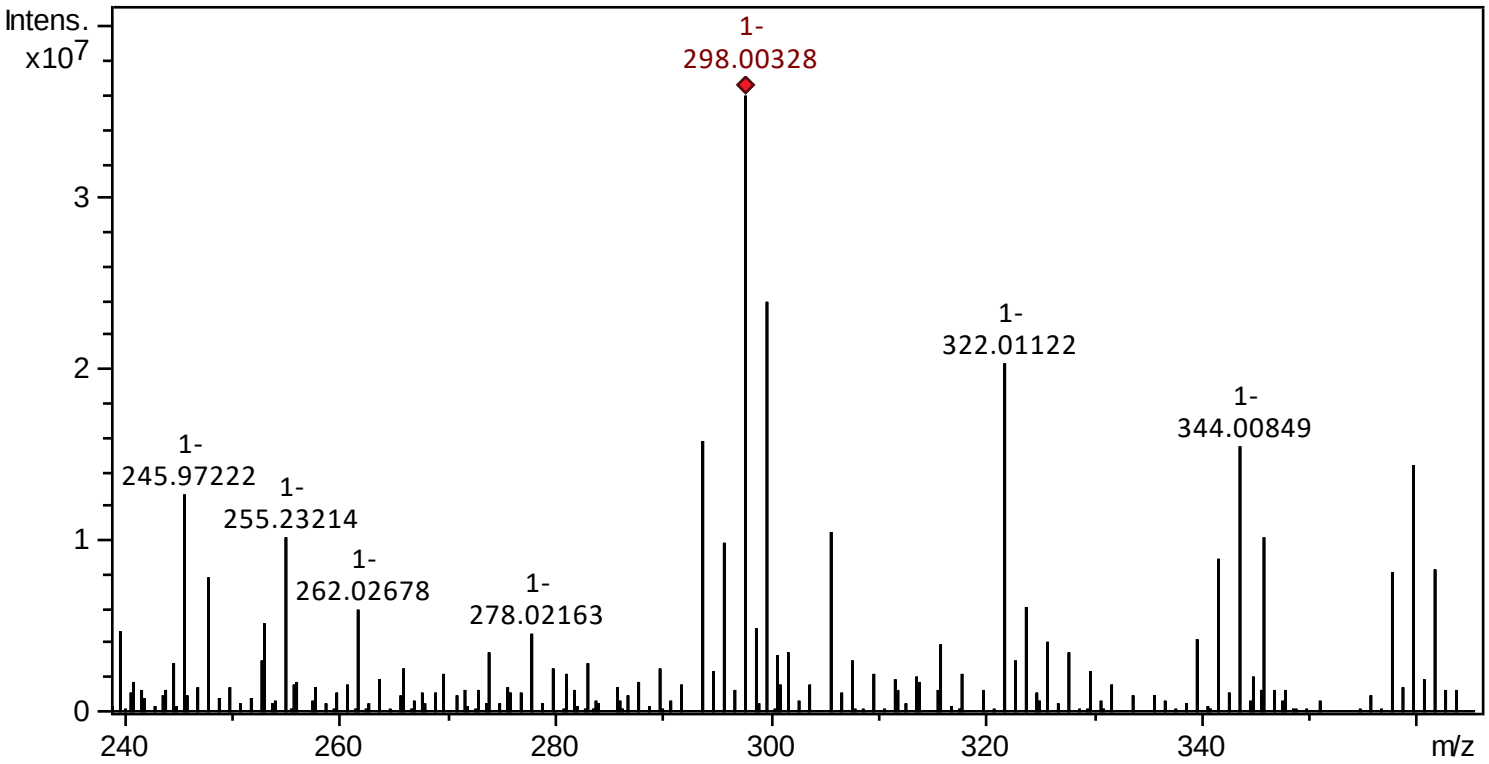

Figure S6. MS spectrum of the oxidation product 2e (m/z 298,0032).

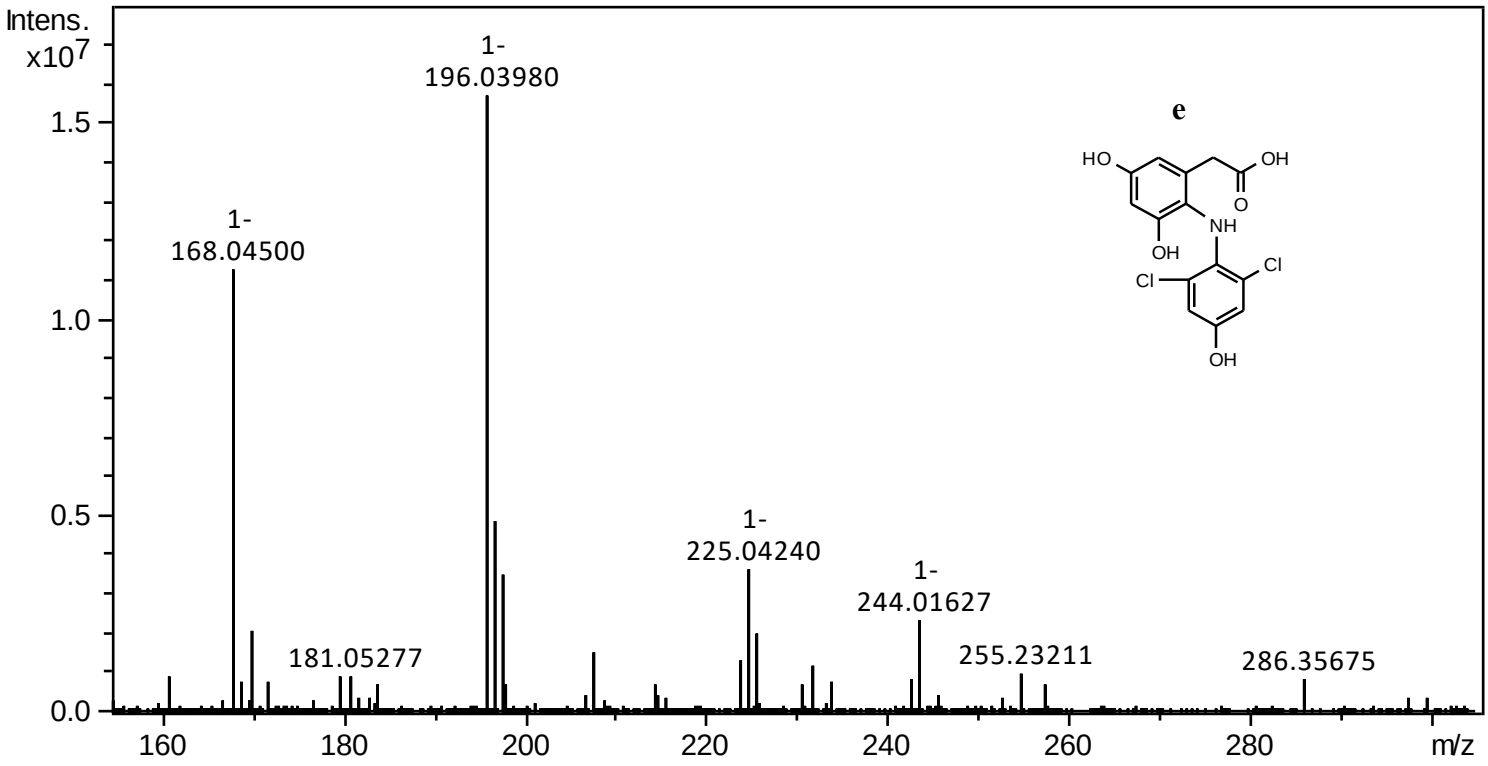

Figure S6a. MS/MS spectrum of 2e precursor ion and its proposed molecular structure.

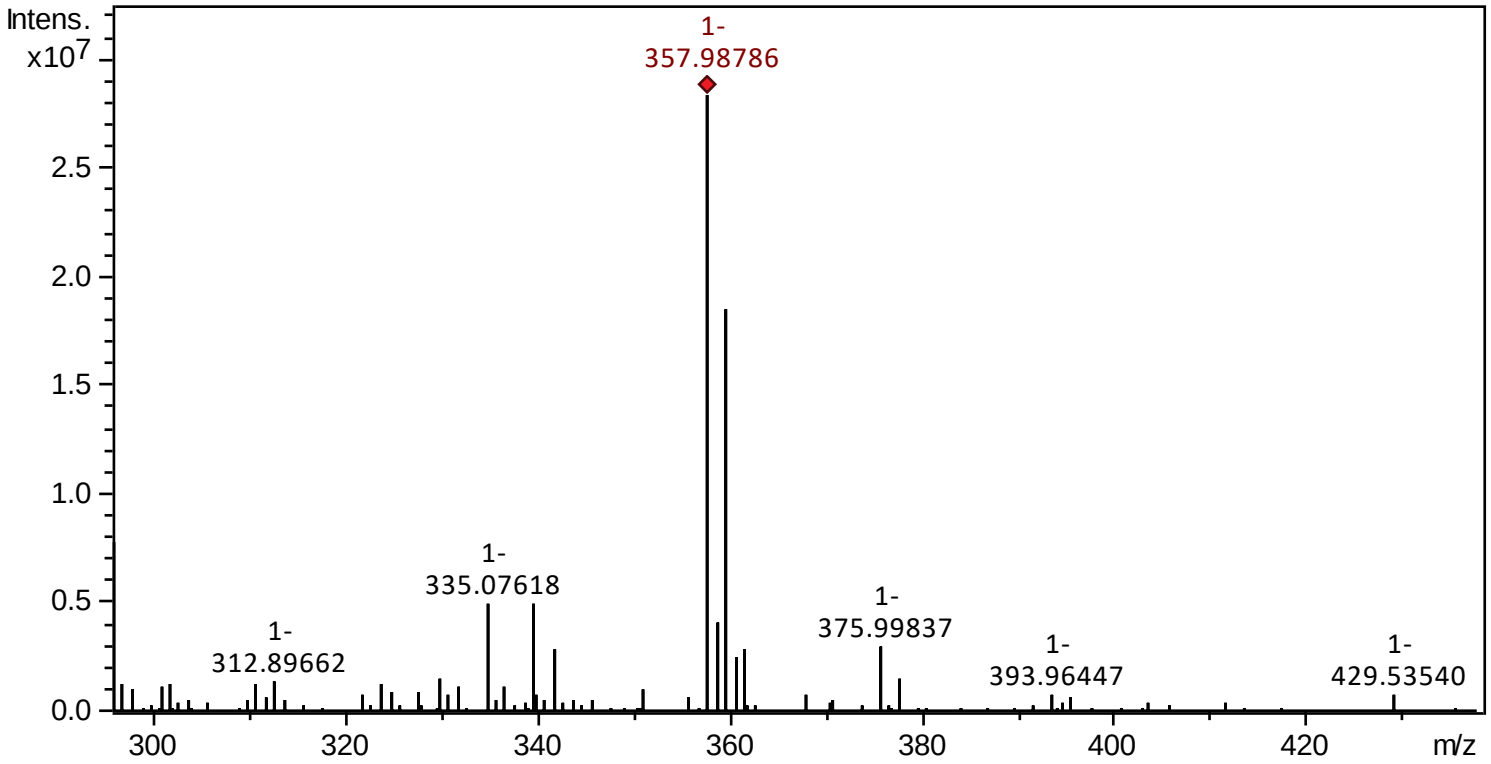

Figure S7. MS spectrum of the oxidation product 2f (m/z 357,9878).

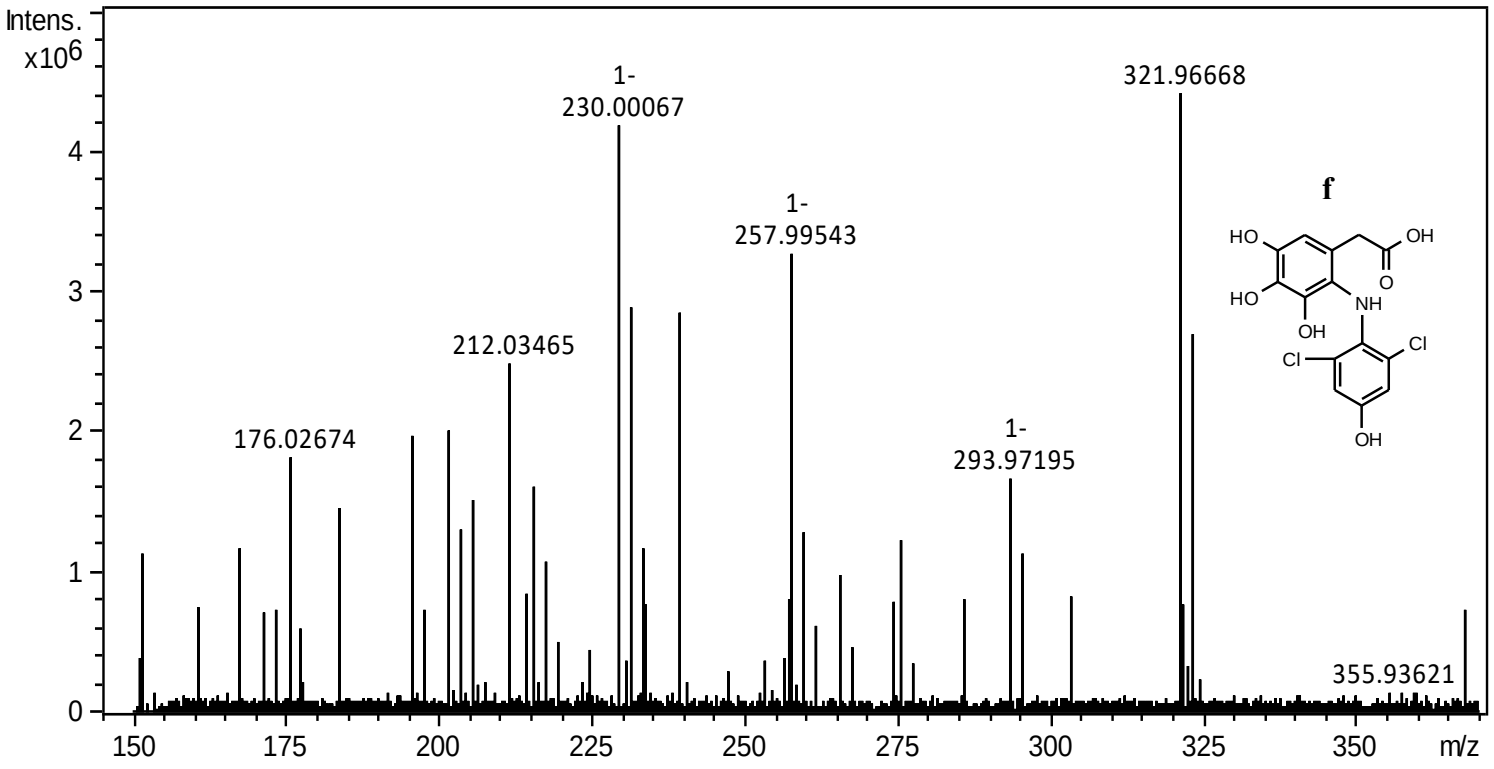

Figure S7a. MS/MS spectrum of 2f precursor ion and its proposed molecular structure.

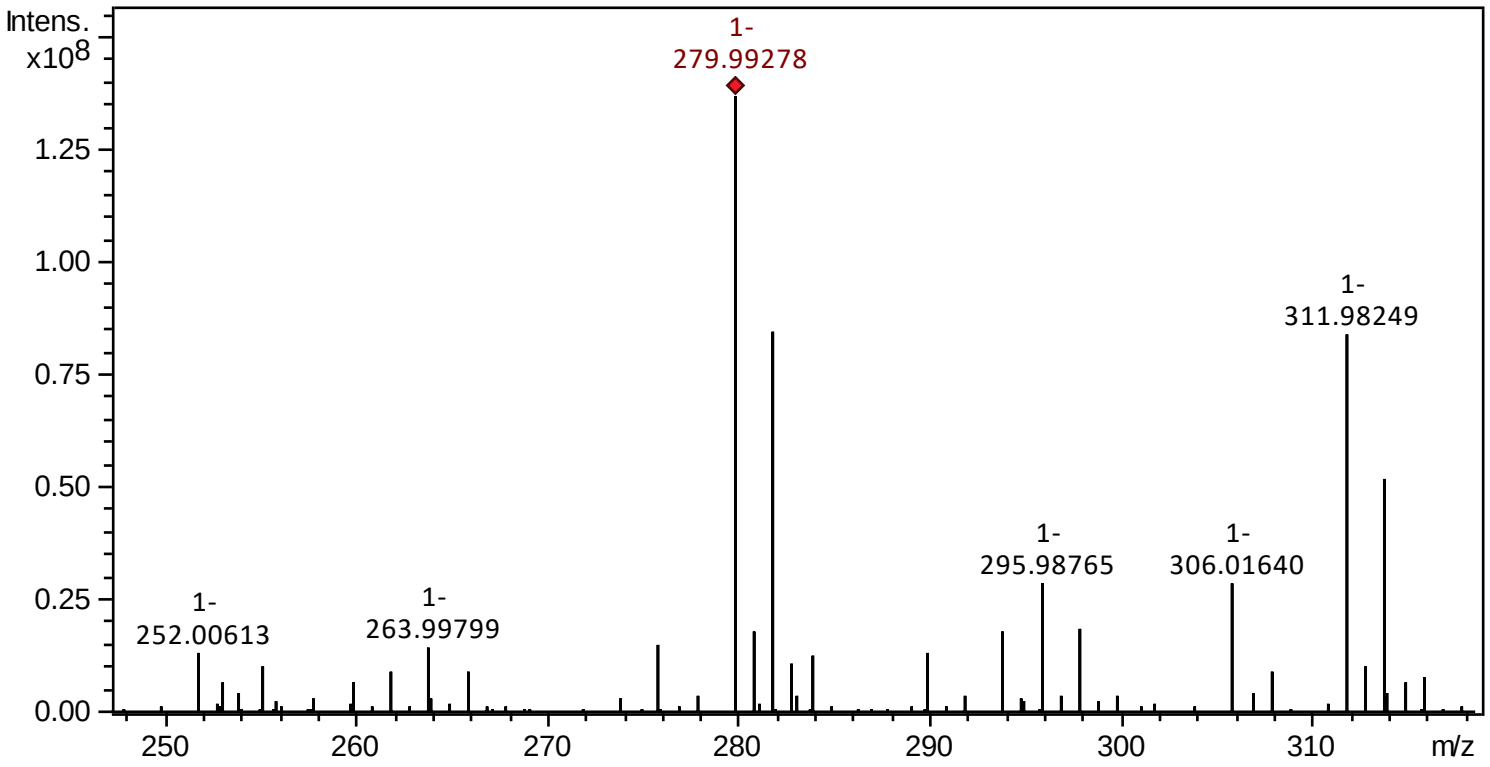

Figure S8. MS spectrum of the oxidation product 2g (m/z 279,9927).

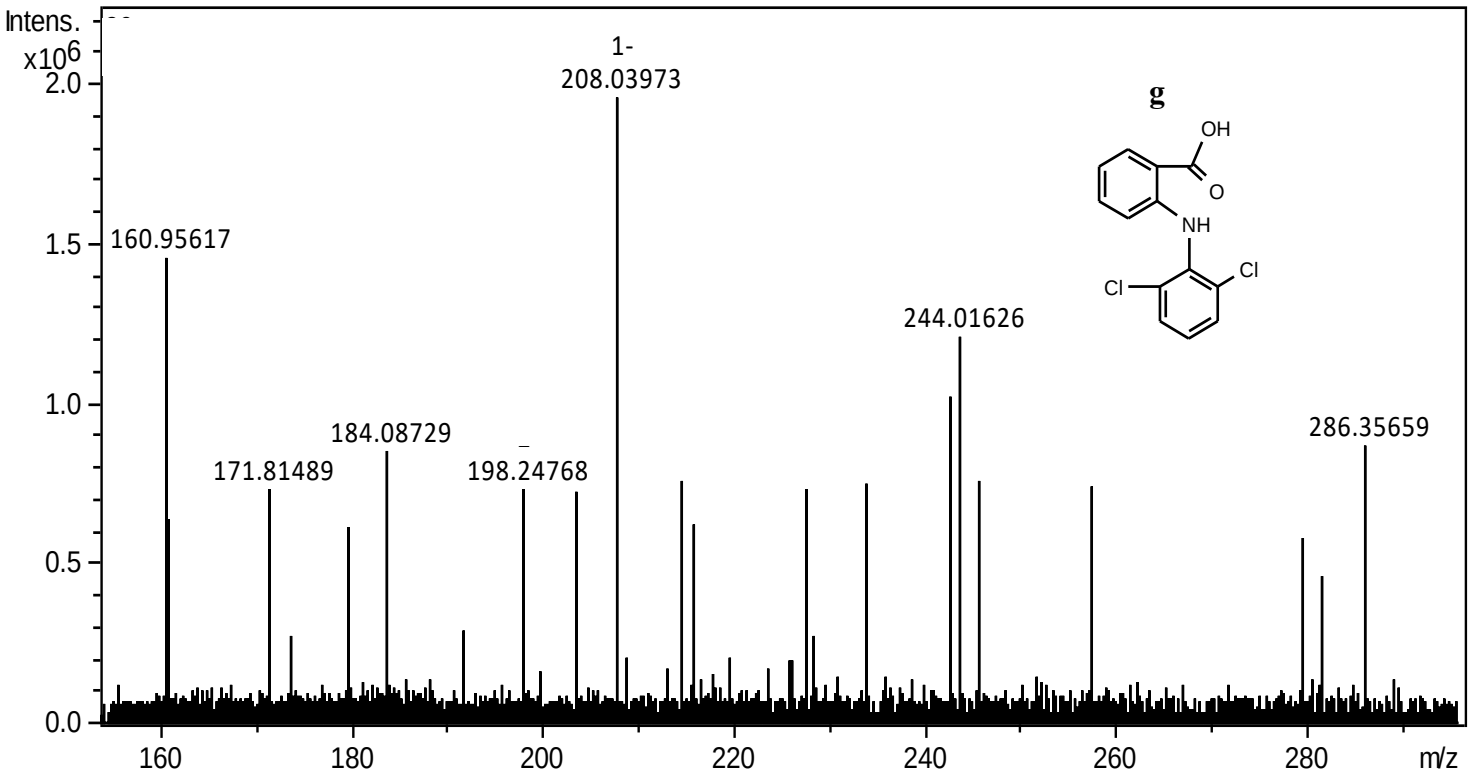

Figure S8a. MS/MS spectrum of 2g precursor ion and its proposed molecular structure.

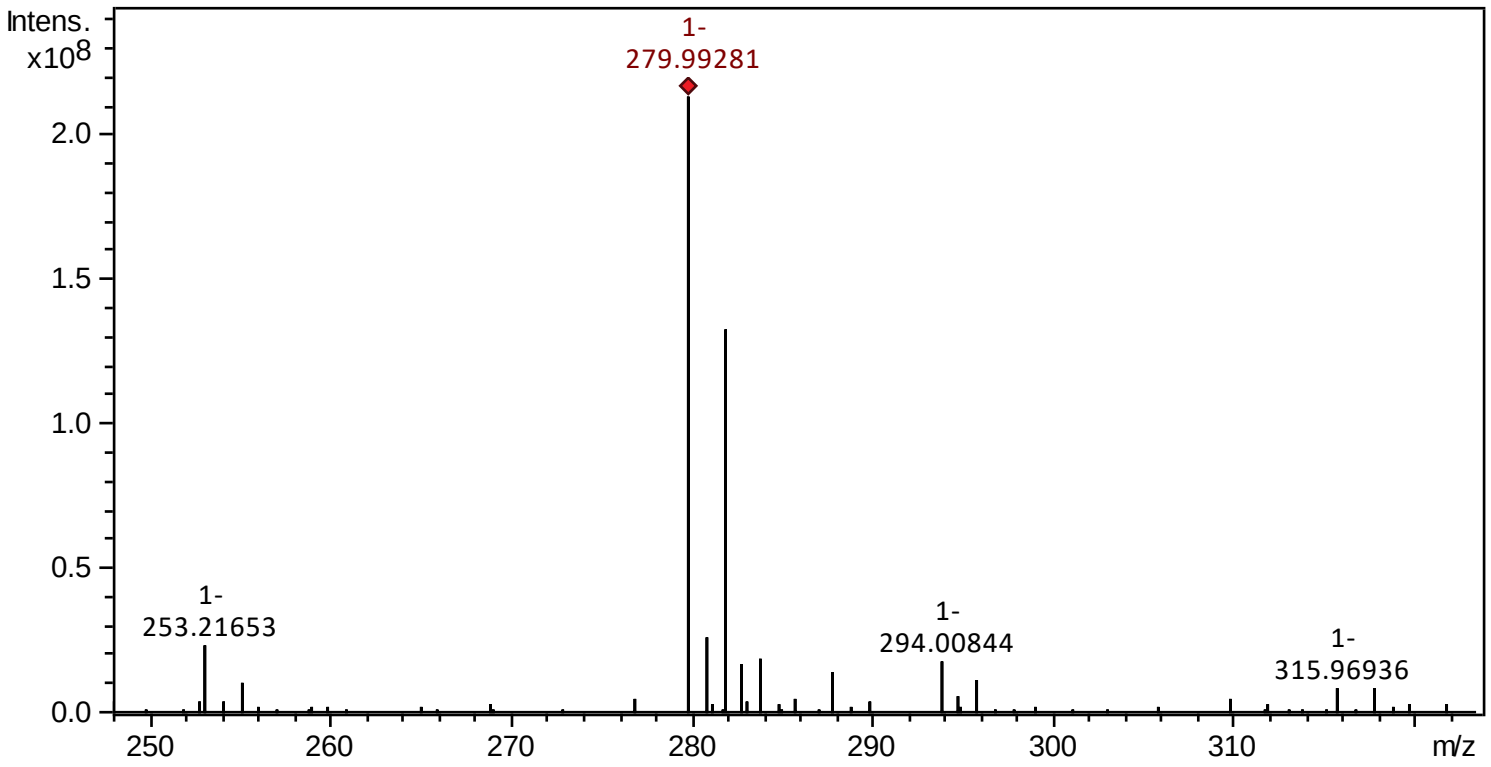

Figure S9. MS spectrum of the oxidation product 2h (m/z 279,9928).

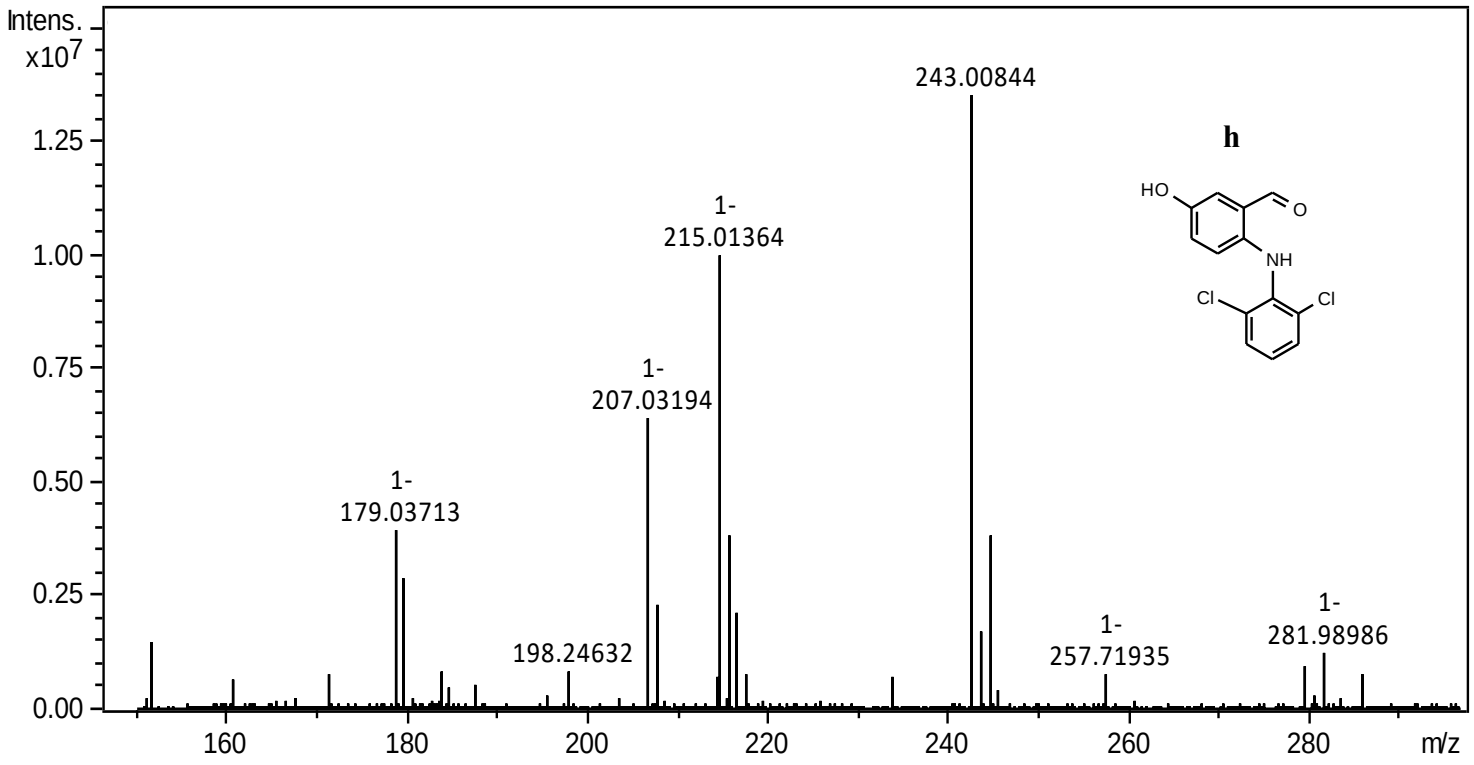

Figure S9a. MS/MS spectrum of 2h precursor ion and its proposed molecular structure.

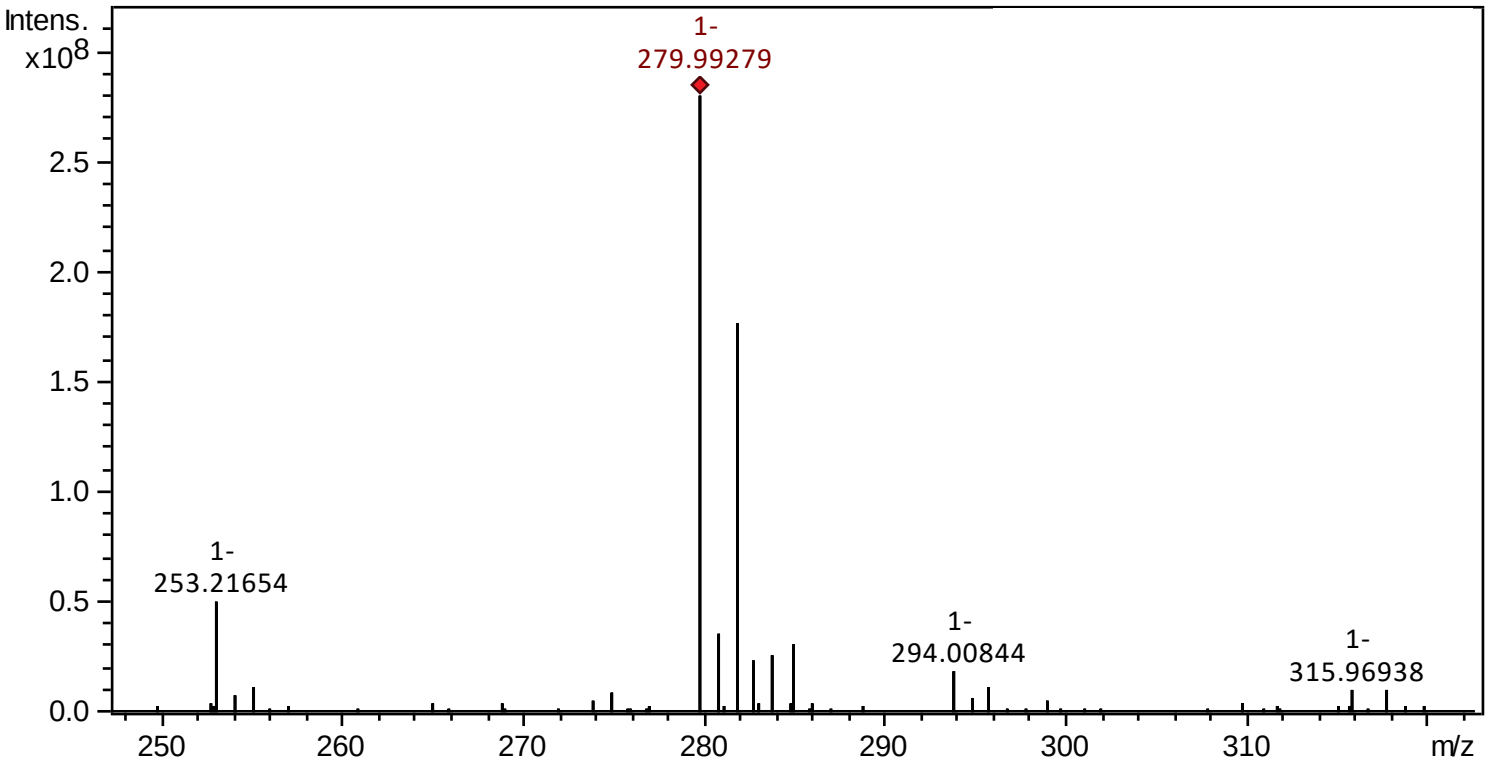

Figure S10. MS spectrum of the oxidation product 2i (m/z 279,9927).

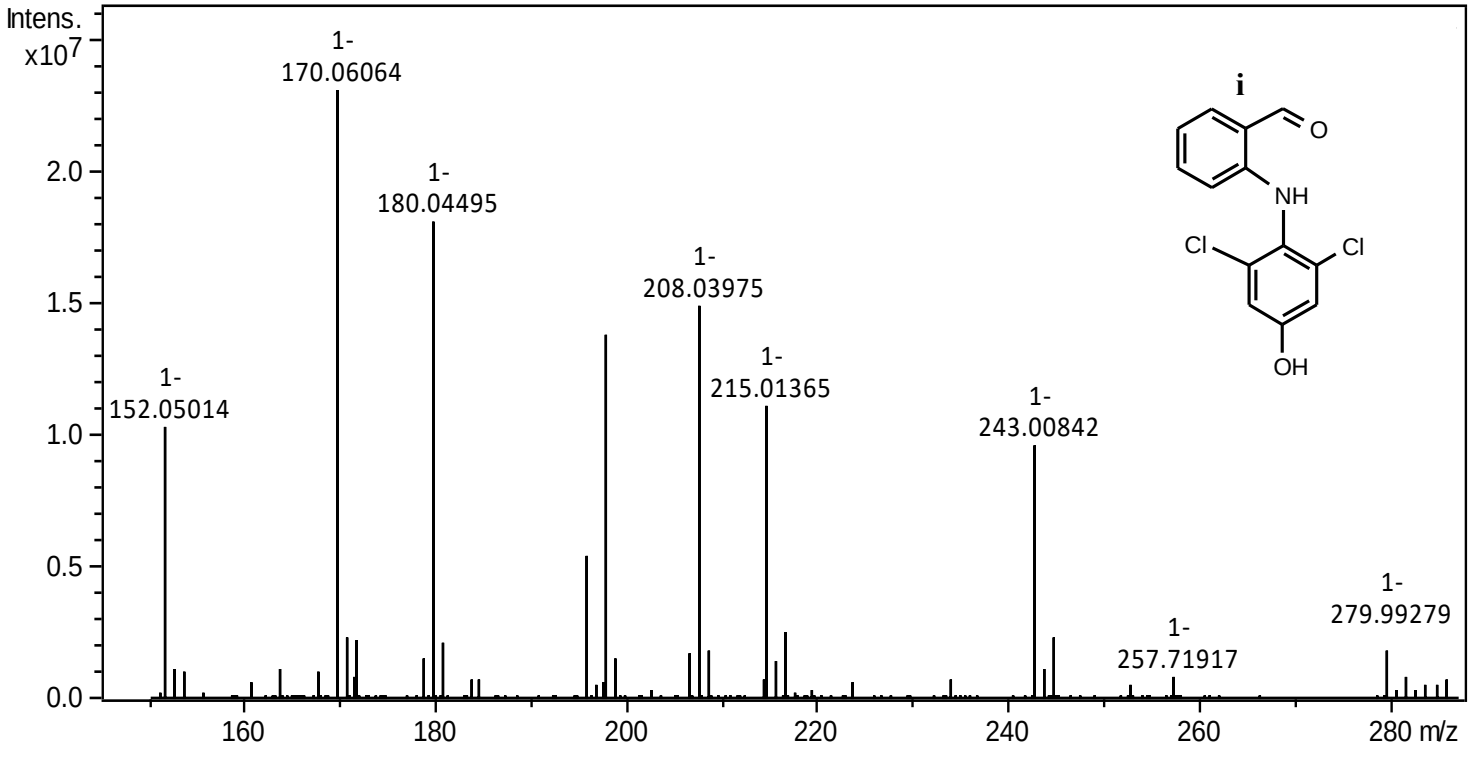

Figure S10a. MS/MS spectrum of 2i precursor ion and its proposed molecular structure.

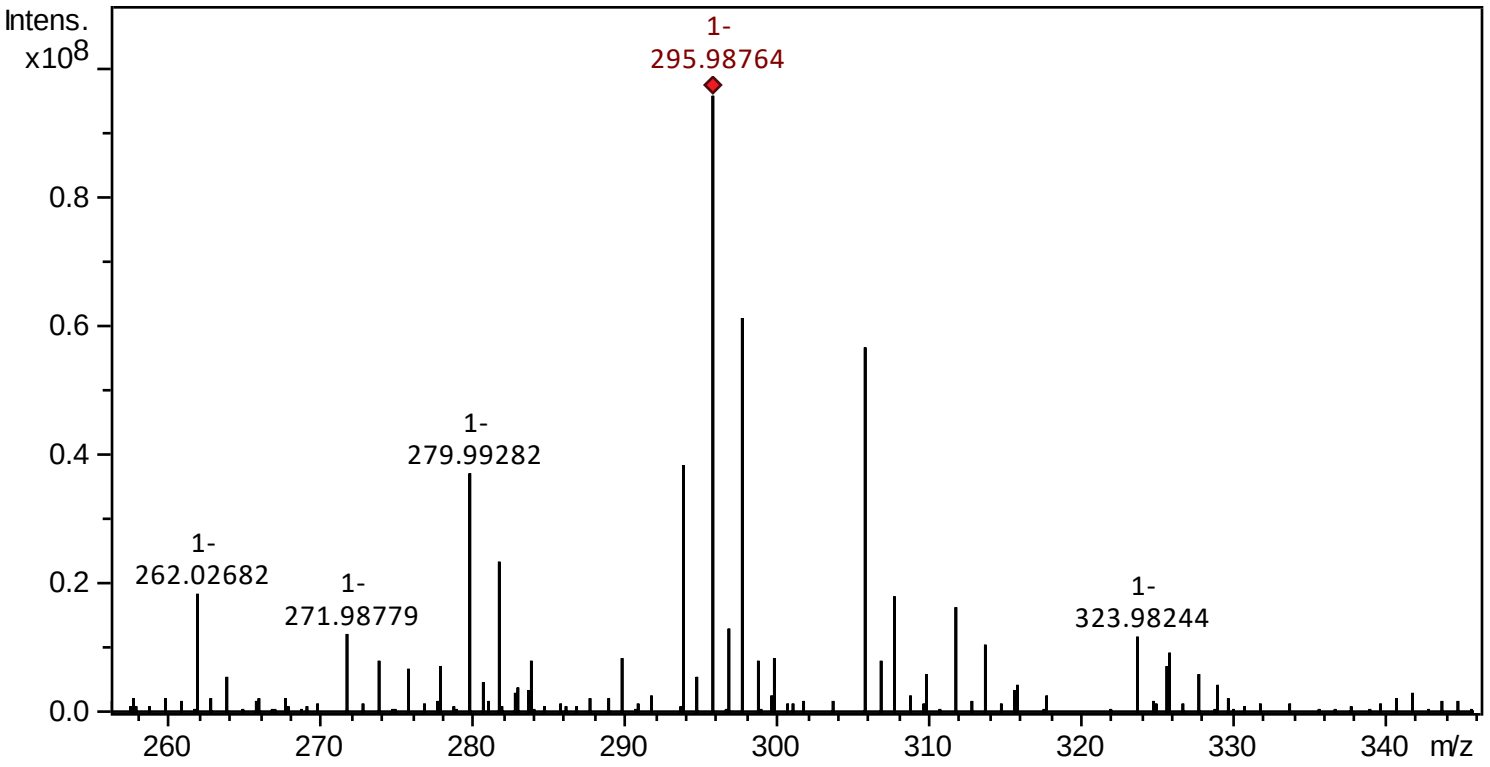

Figure S11. MS spectrum of the oxidation product 2j (m/z 295,9876).

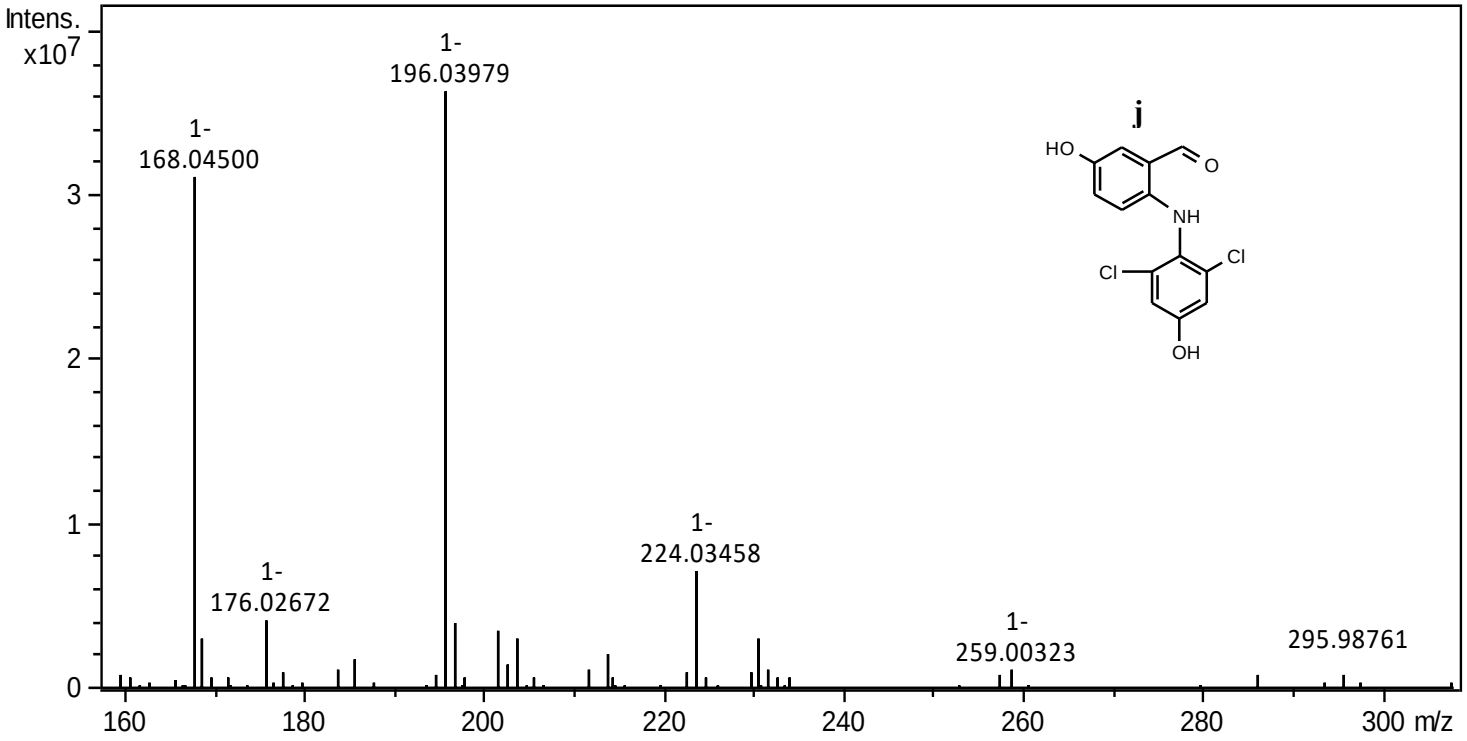

Figure S11a. MS/MS spectrum of 2j precursor ion and its proposed molecular structure.

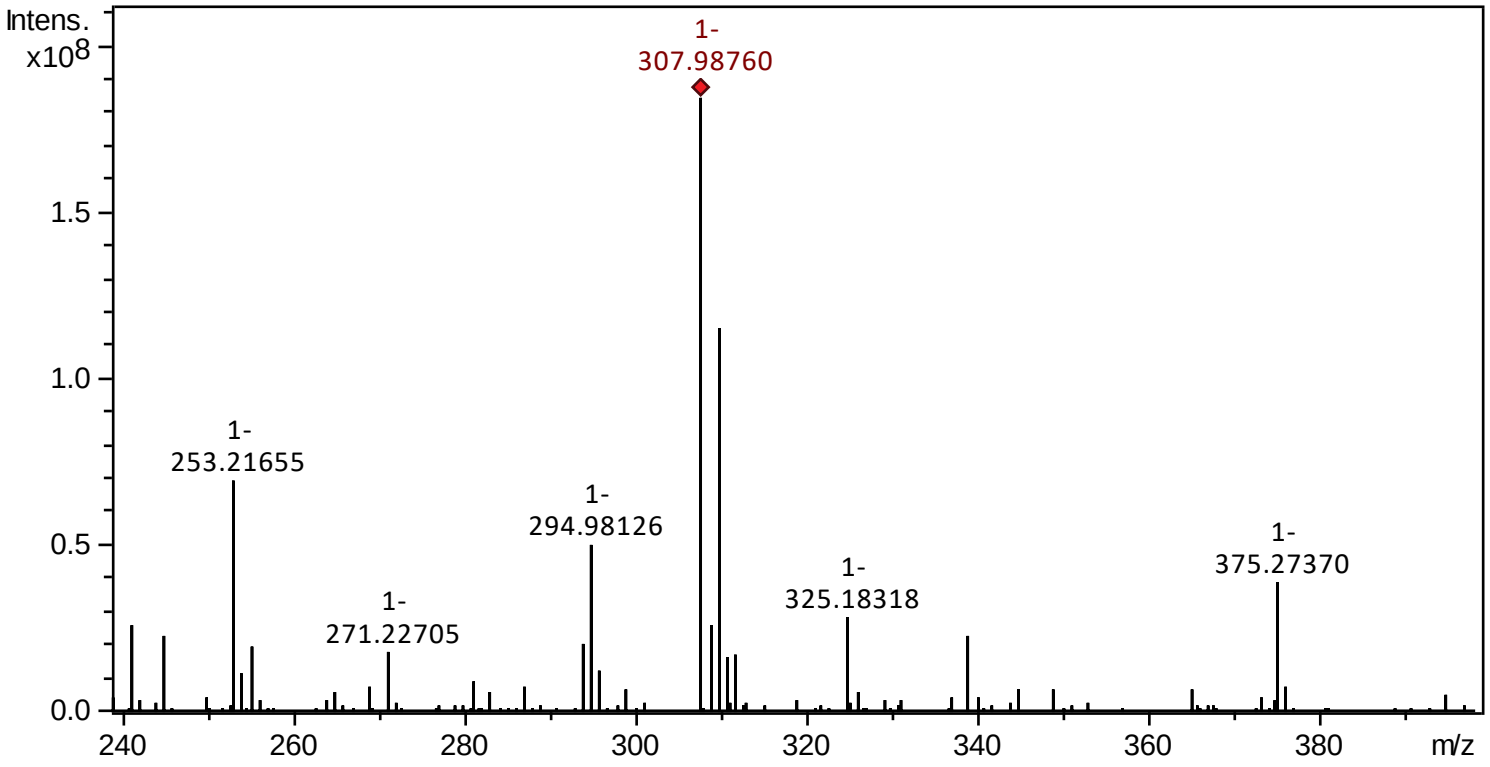

Figure S12. MS spectrum of the oxidation product 3a (m/z 307,9876).

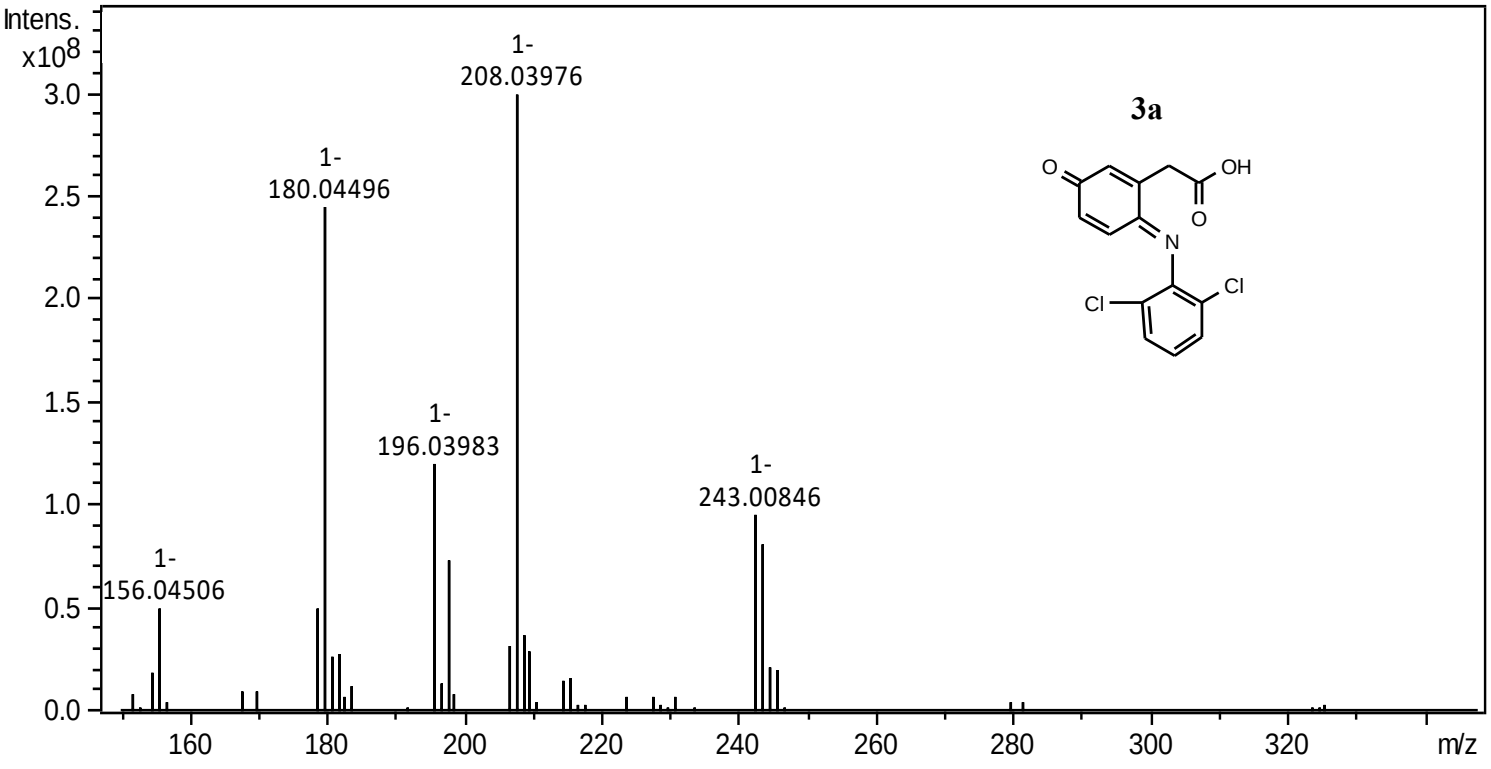

Figure S12a. MS/MS spectrum of 3a precursor ion and its proposed molecular structure.

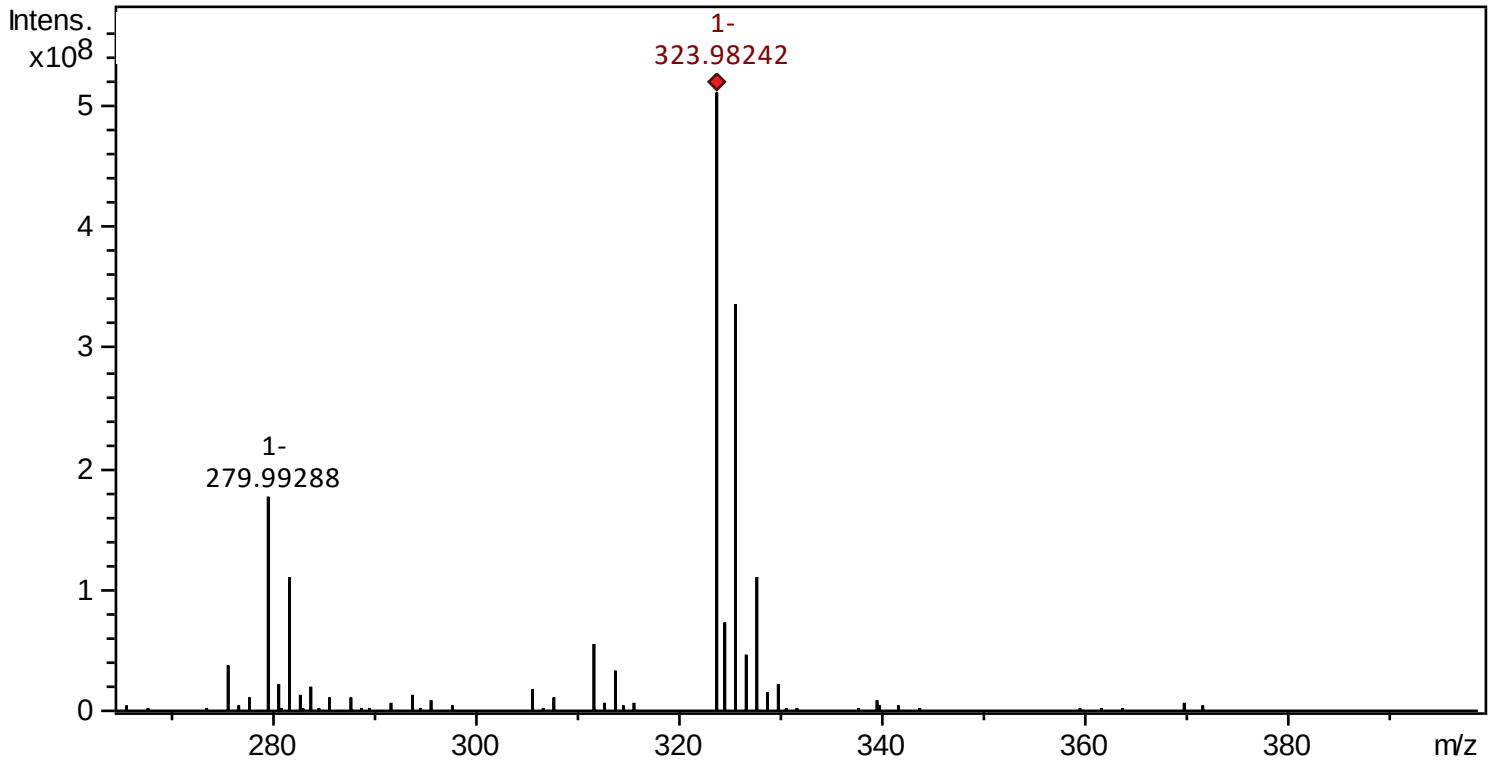

Figure S13. MS spectrum of the oxidation product 3b (m/z 323,9824).

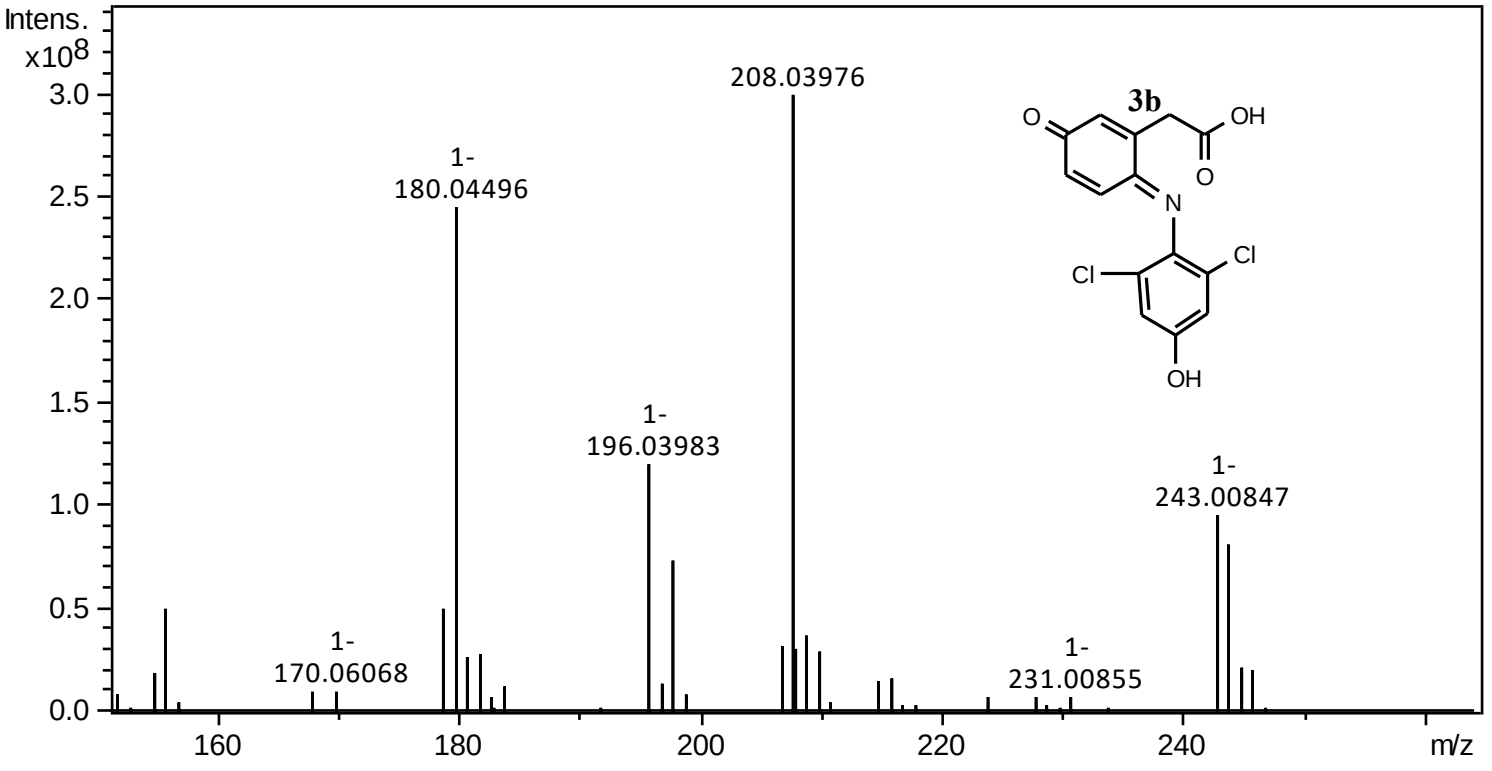

Figure S13a. MS/MS spectrum of 3b precursor ion and its proposed molecular structure.

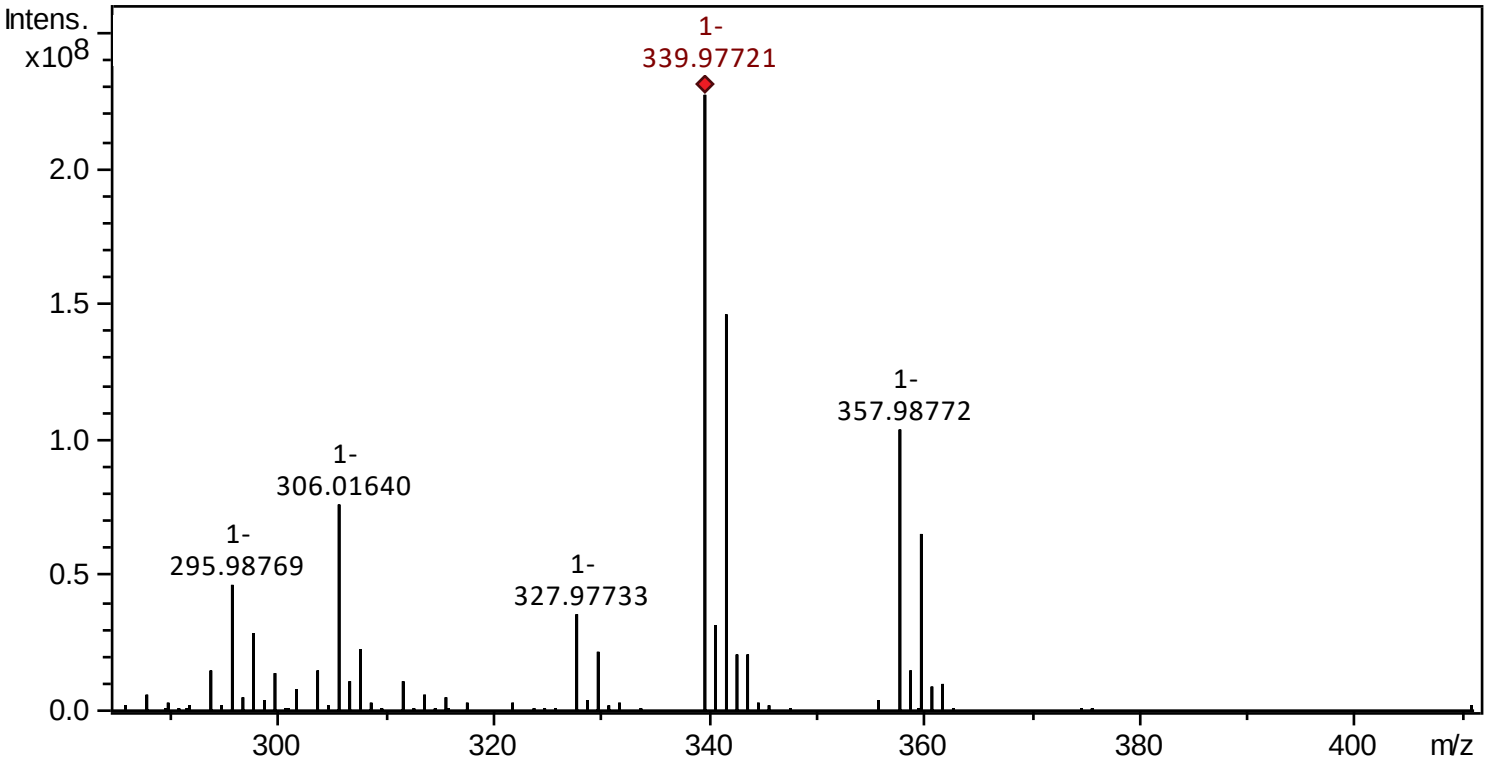

Figure S14. MS spectrum of the oxidation product 3c (m/z 339,9774).

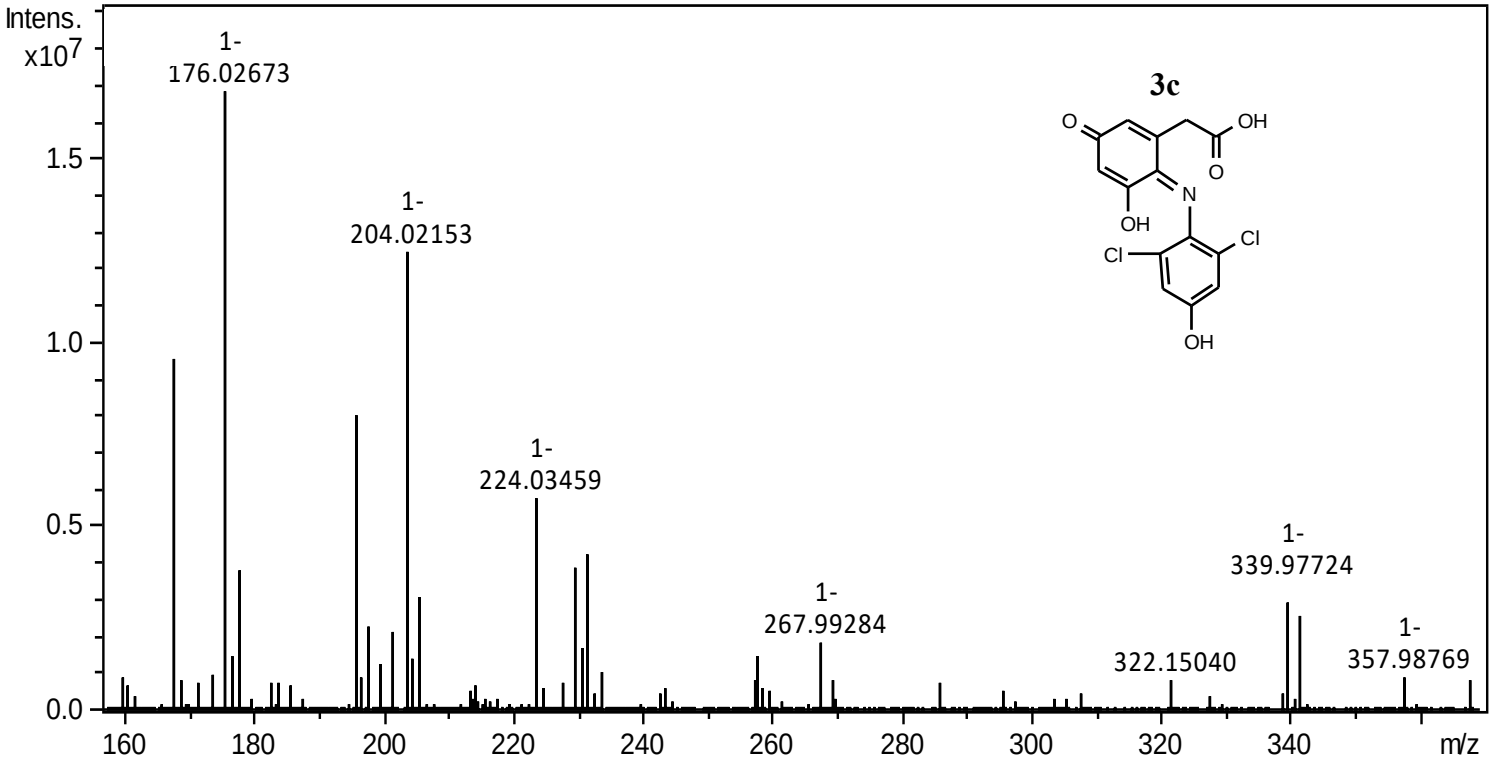

Figure S14a. MS/MS spectrum of 3c precursor ion and its proposed molecular structure.

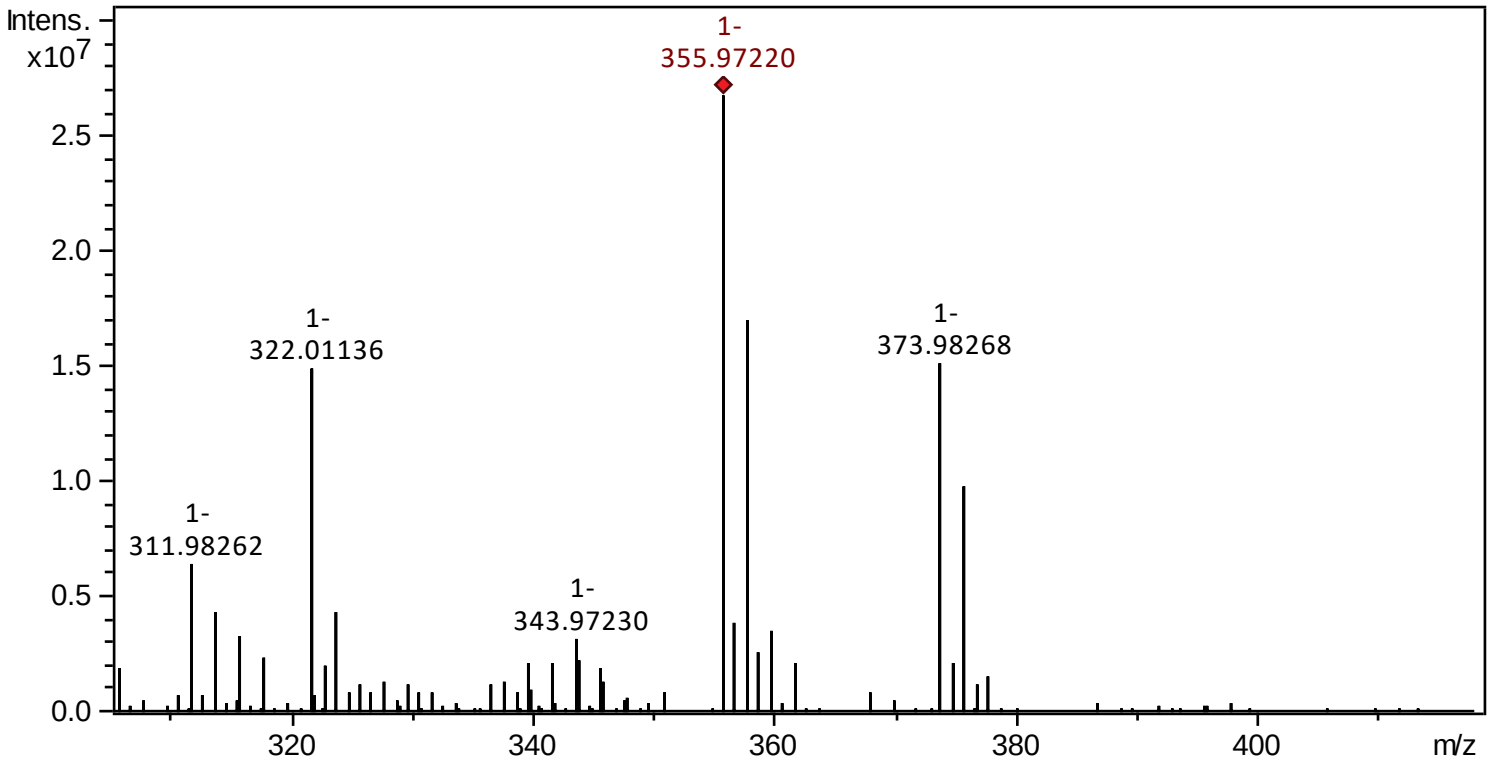

Figure S15. MS spectrum of the oxidation product 3d (m/z 355,9722).

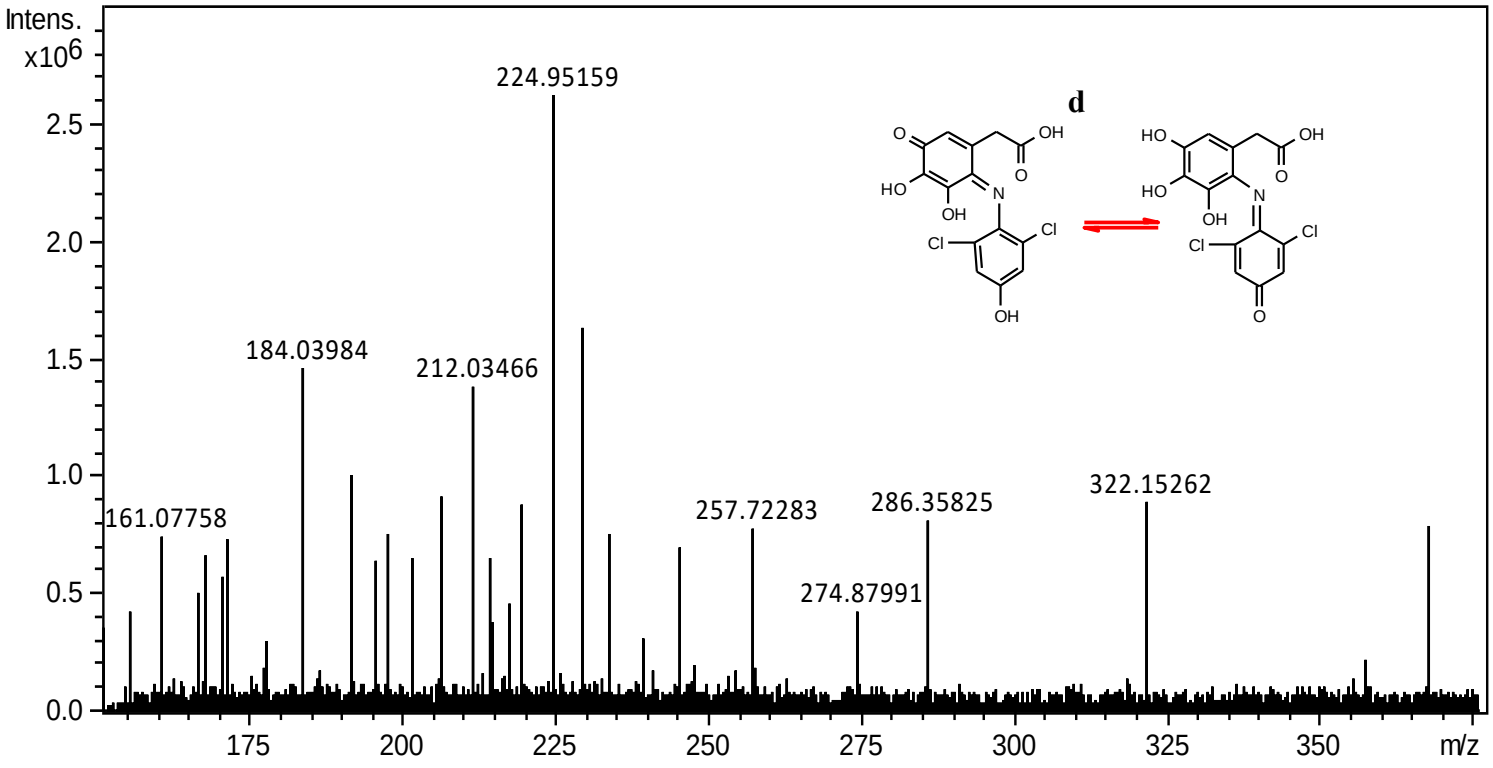

Figure S15a. MS/MS spectrum of 3d precursor ion and its proposed molecular structure.

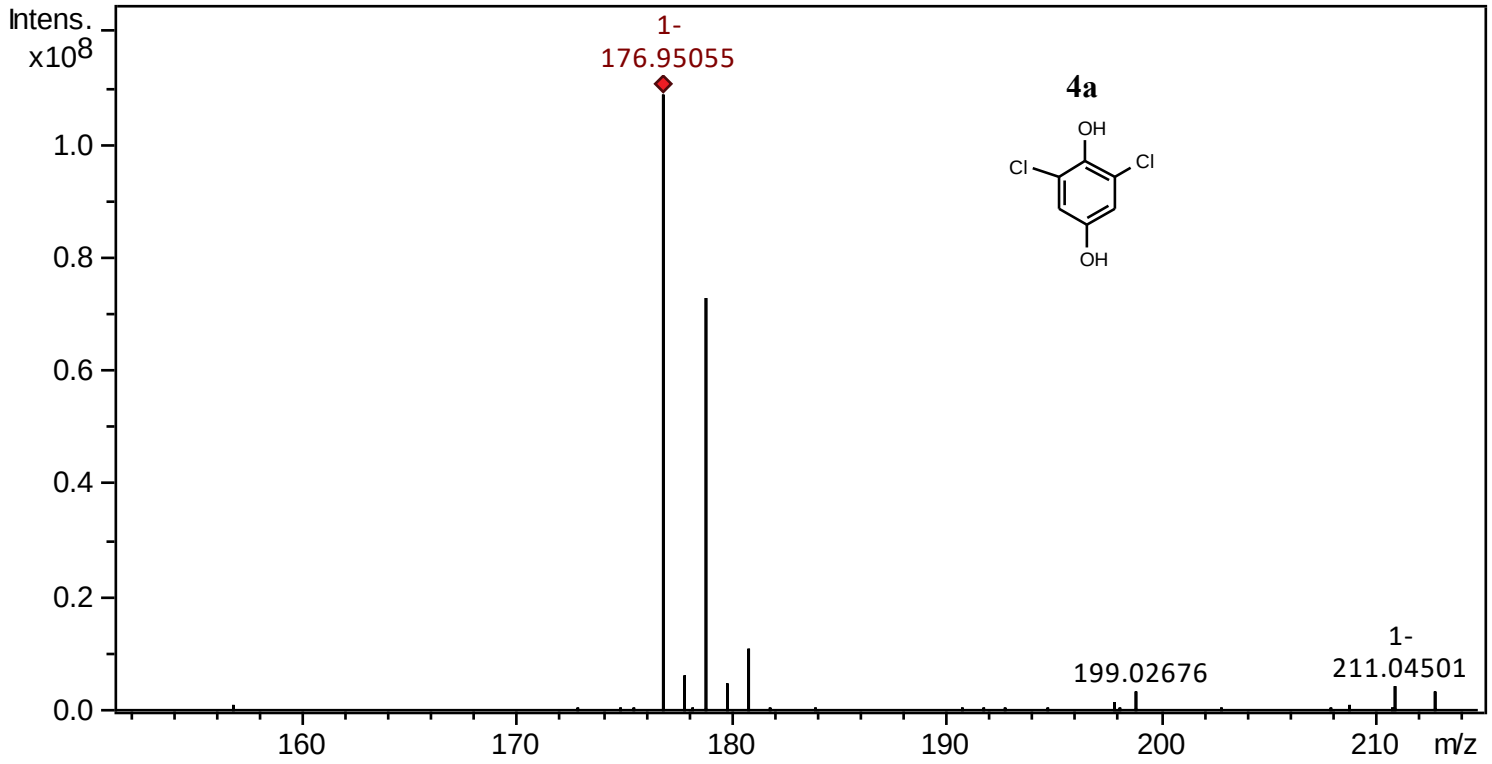

Figure S16. MS spectrum of the oxidation product 4a (m/z 176,9505) and its proposed molecular structure.

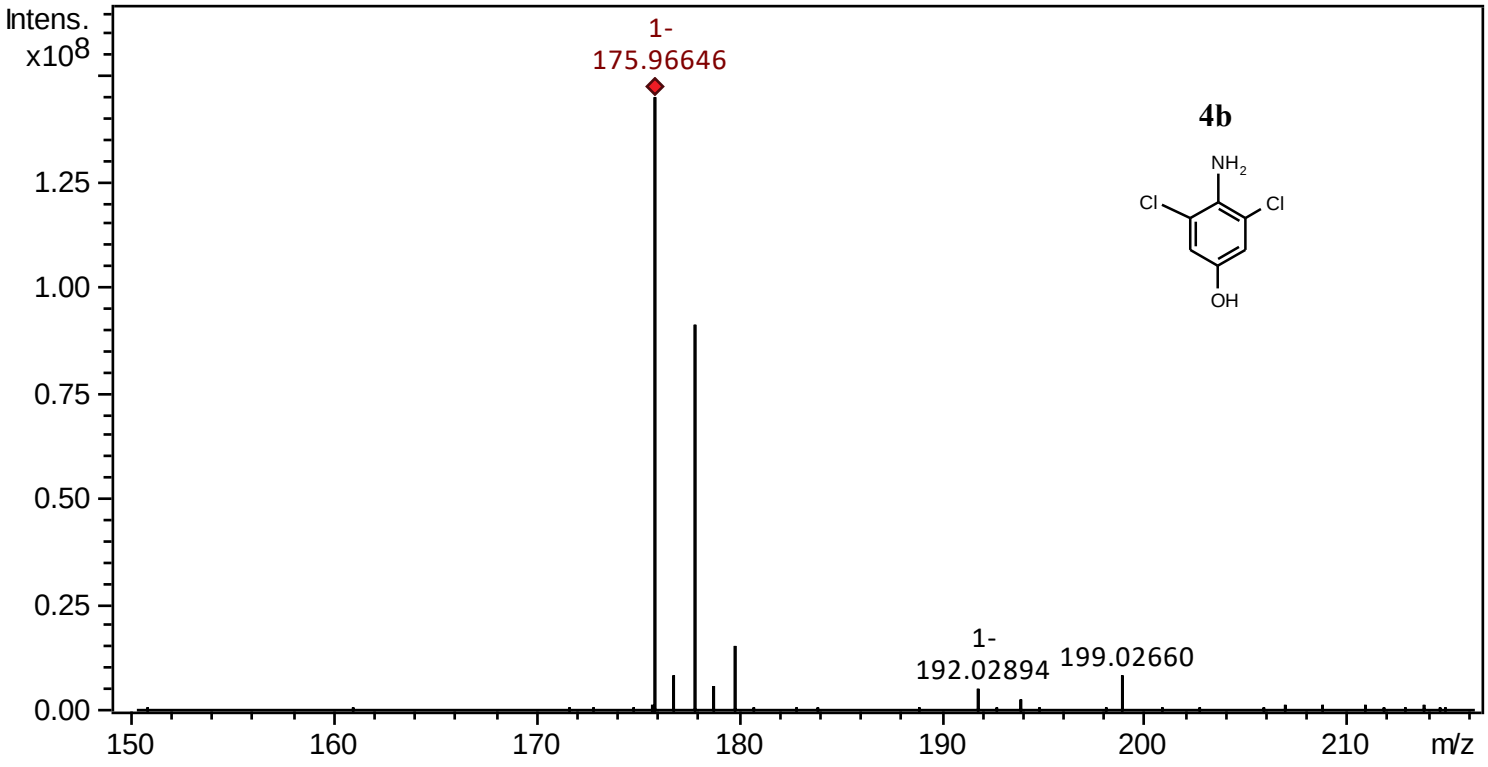

Figure S17. MS spectrum of the oxidation product 4b (m/z 175,9664) and its proposed molecular structure.

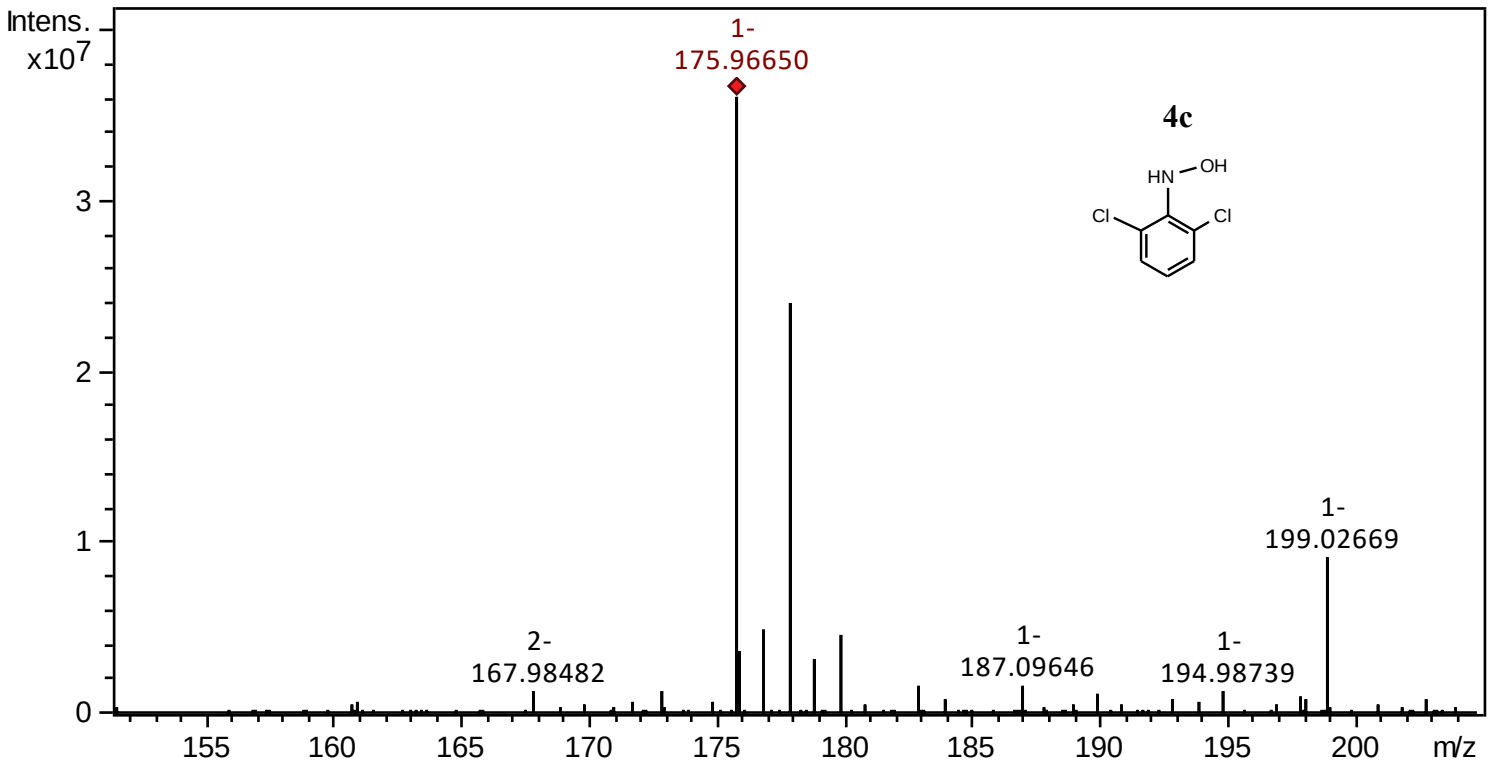

Figure S18. MS spectrum of the oxidation product 4c (m/z 175,9665) and its proposed molecular structure.

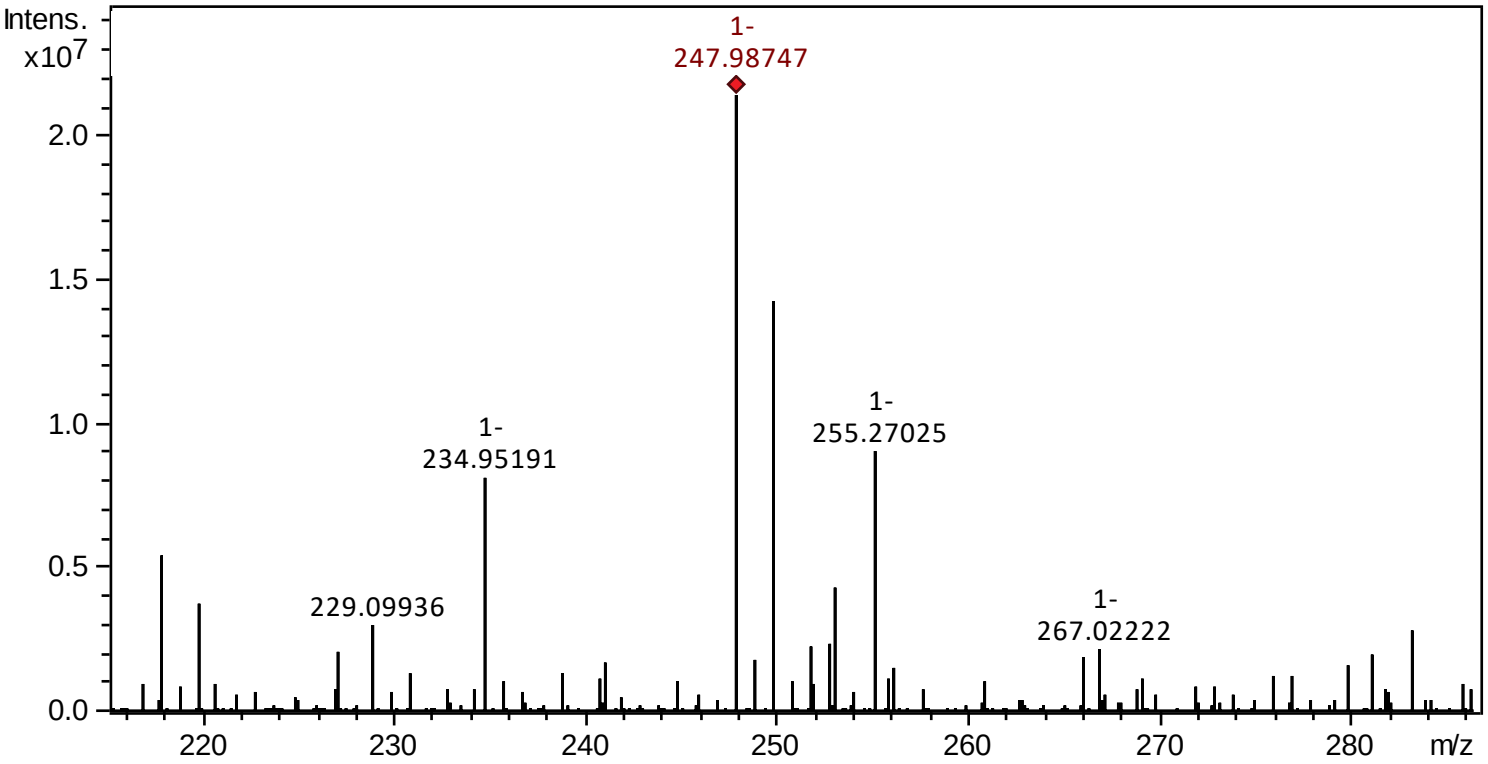

Figure S19. MS spectrum of the oxidation product 4d (m/z 247,9874).

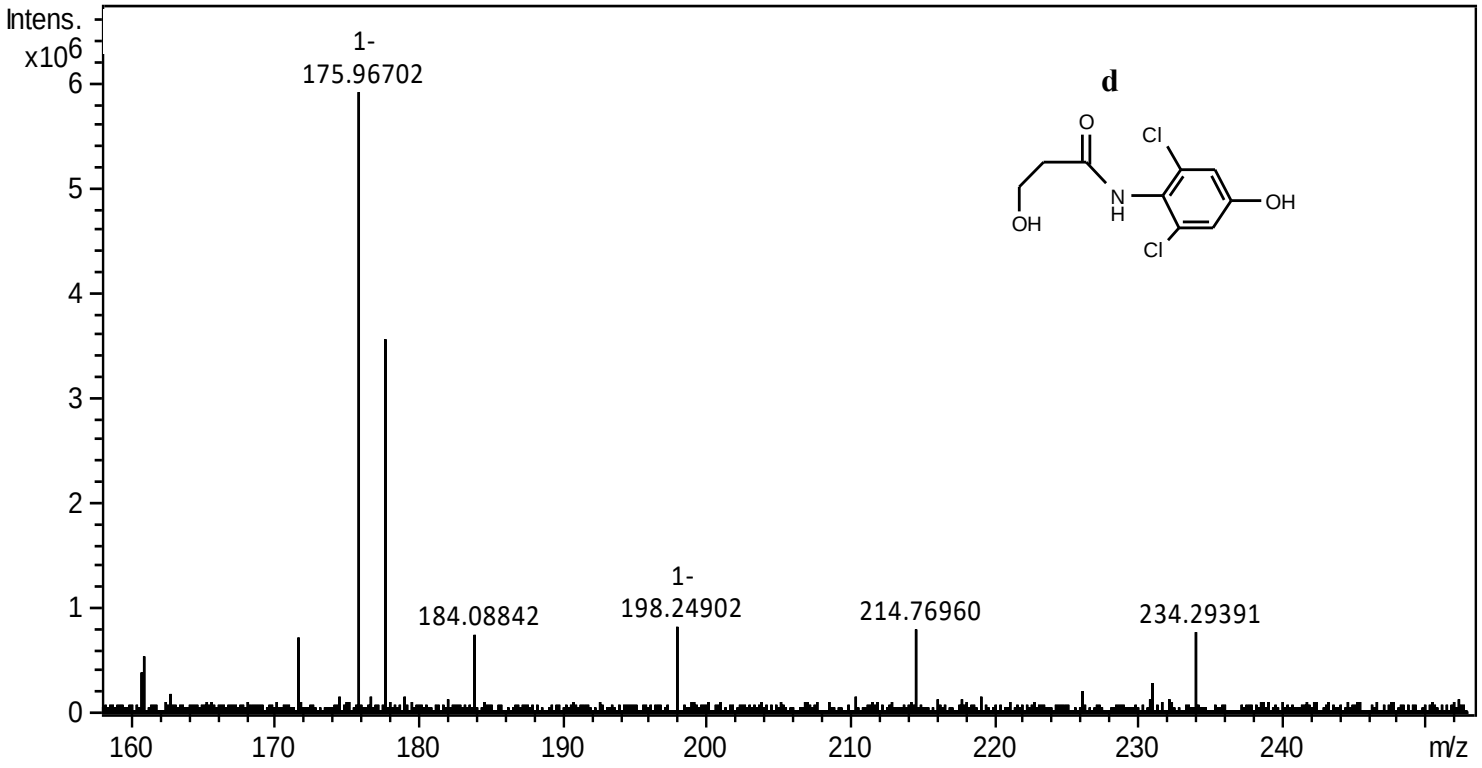

Figure S19a. MS/MS spectrum of 4d precursor ion and its proposed molecular structure.

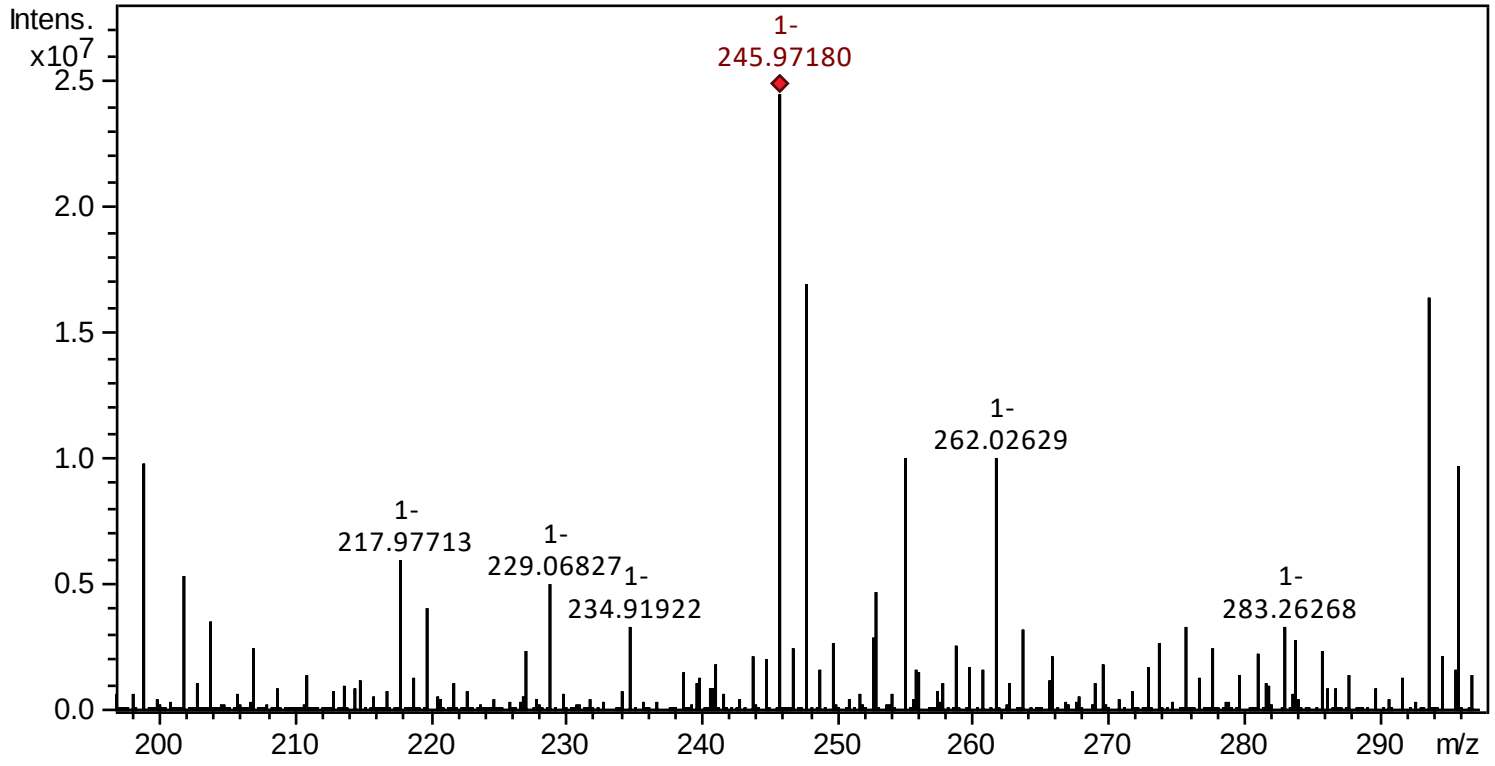

Figure S20. MS spectrum of the oxidation product 4e (m/z 245,9718).

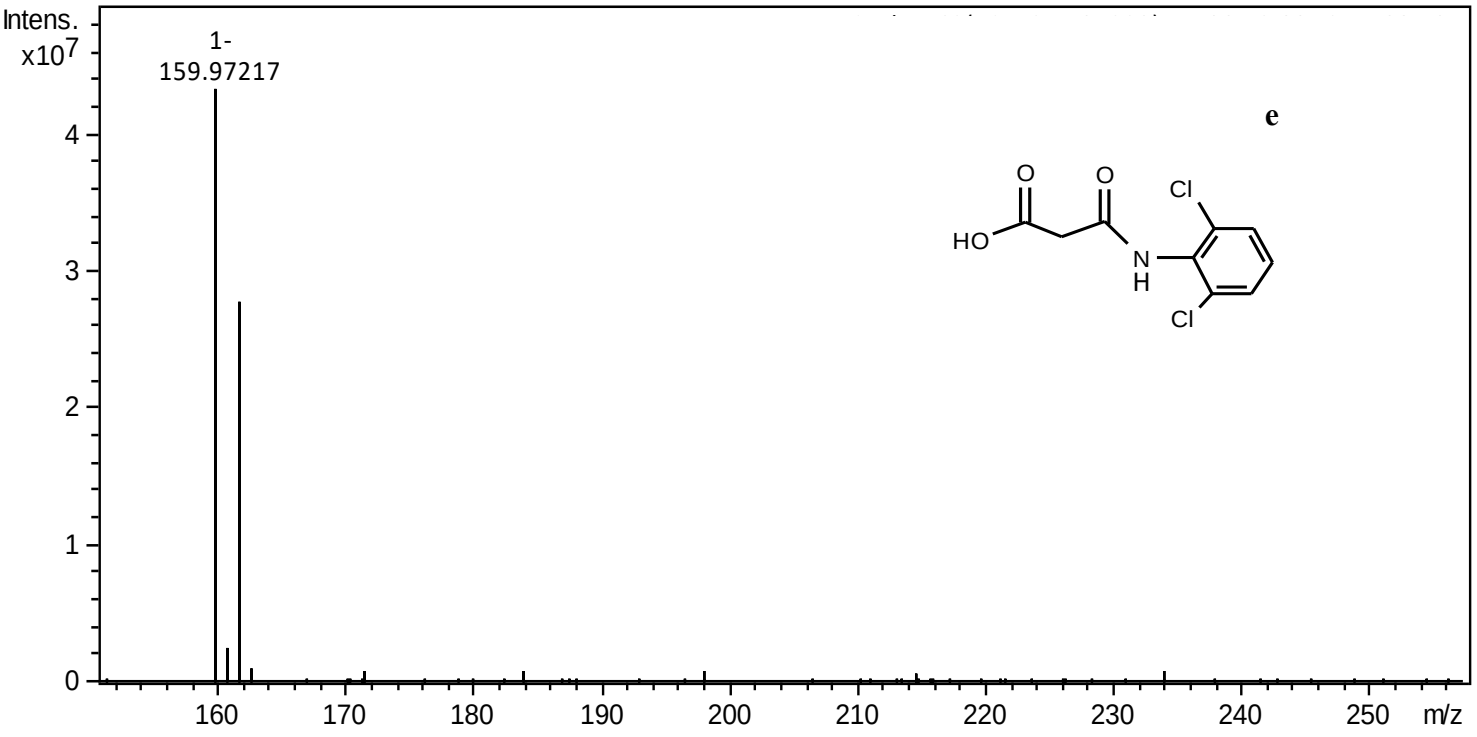

Figure S20a. MS/MS spectrum of 4e precursor ion and its proposed molecular structure.

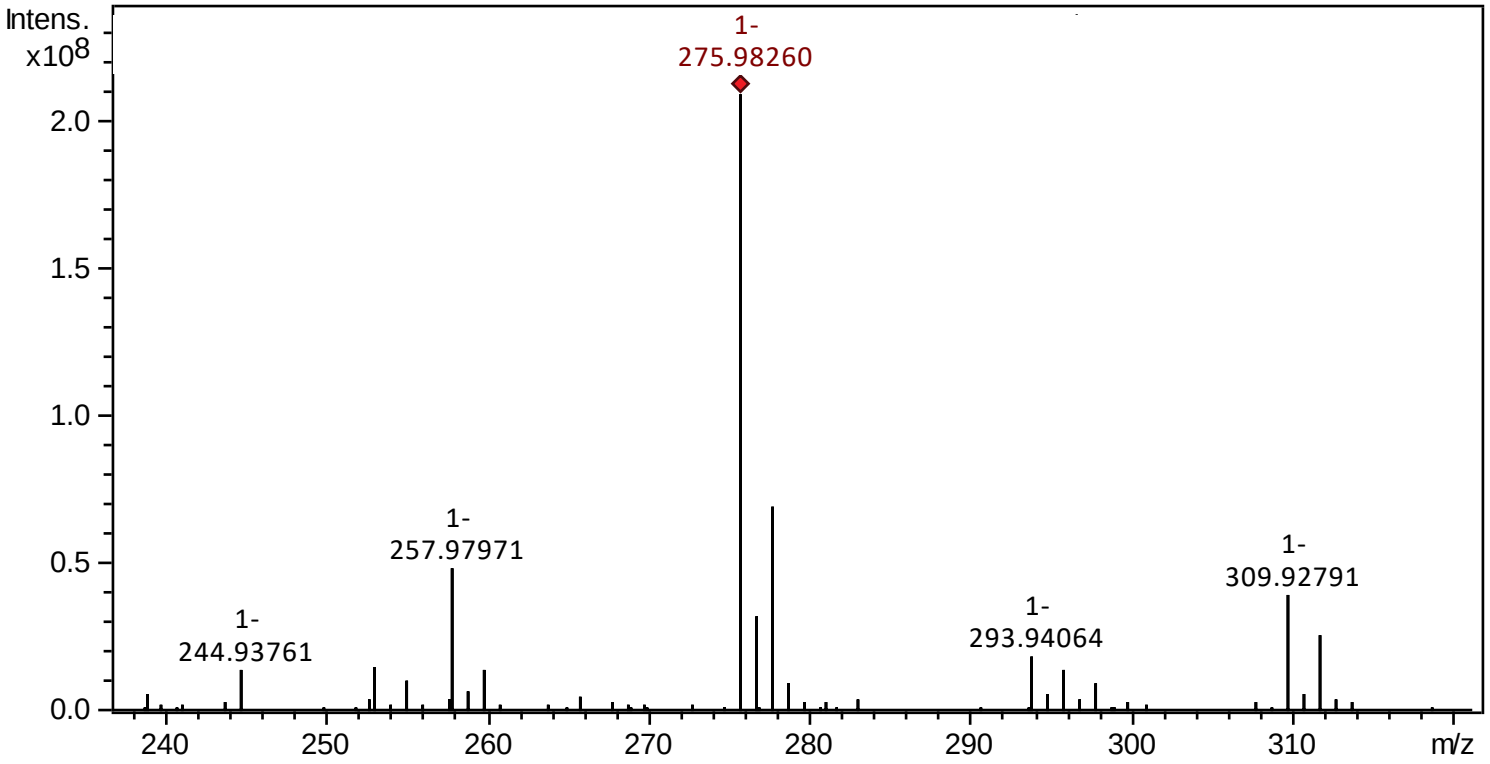

Figure S21. MS spectrum of the oxidation product 4f (m/z 275,9826).

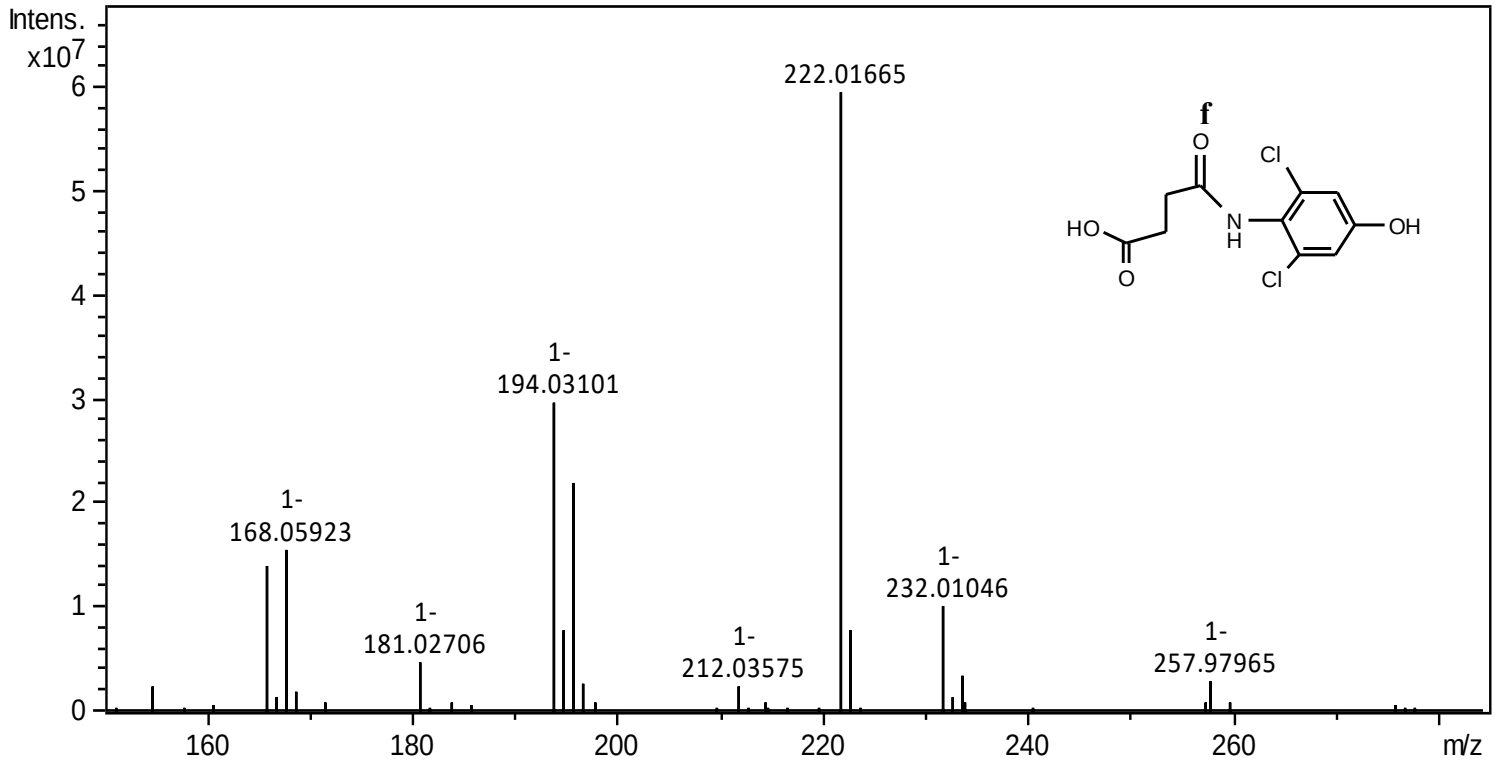

Figure S21a. MS/MS spectrum of 4f precursor ion and its proposed molecular structure.

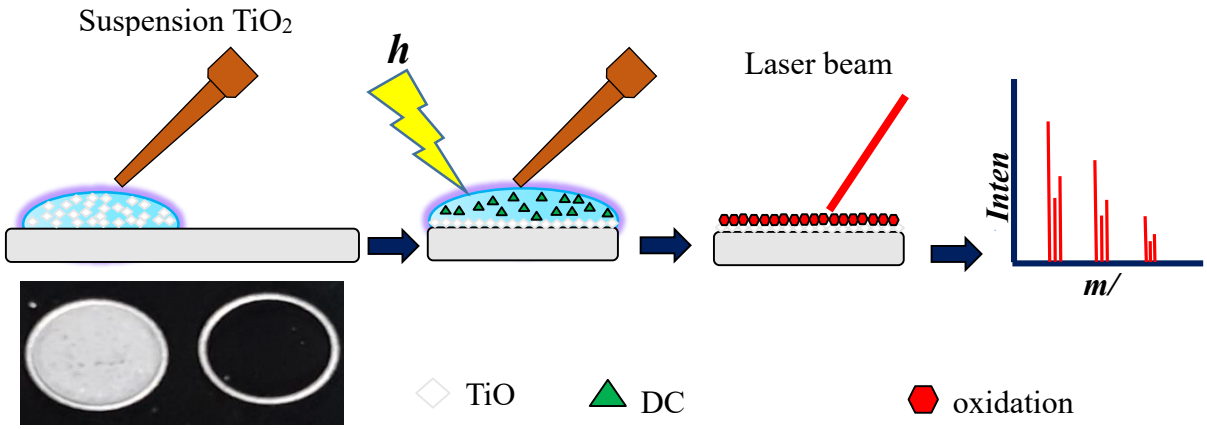

Figure S22. Schematic representation of «on-target» UV/TiO_2-PCO.